

1
2
3
4
5
6
7
8
9
10
11
12
13
14
15
16
17
18
19
20
21
22
23
24
25
26
27
28
29
30

Phase, composition and growth mechanism for secondary organic aerosol from the
ozonolysis of α -cedrene

Yue Zhao, Lisa M. Wingen, Veronique Perraud, and Barbara J. Finlayson-Pitts*

Department of Chemistry
University of California
Irvine, CA 92697, USA

*Corresponding author: Email: bjfinlay@uci.edu; phone: (949) 824-7670; Fax: (949) 824-2420

31 **Abstract**

32 Sesquiterpenes are an important class of biogenic volatile organic compounds (BVOCs) and
33 have a high secondary organic aerosol (SOA) forming potential. However, SOA formation from
34 sesquiterpene oxidation has received less attention compared to other BVOCs such as
35 monoterpenes, and the underlying mechanisms remain poorly understood. In this work, we
36 present a comprehensive experimental investigation of the ozonolysis of α -cedrene both in a
37 glass flow reactor (27-44 s reaction times) and in static Teflon chambers (30-60 min reaction
38 times). The SOA was collected by impaction or filters, followed by analysis using attenuated
39 total reflectance-Fourier transform infrared spectroscopy (ATR-FTIR) and electrospray
40 ionization mass spectrometry (ESI-MS), or measured on line using direct analysis in real time
41 (DART-MS) and aerosol mass spectrometry (AMS). The slow evaporation of 2-ethylhexyl
42 nitrate that was incorporated into the SOA during its formation and growth gives an estimated
43 diffusion coefficient of $3 \times 10^{-15} \text{ cm}^2 \text{ s}^{-1}$ and shows that SOA is a highly viscous semi-solid.
44 Possible structures of four newly observed low molecular weight ($\text{MW} \leq 300 \text{ Da}$) reaction
45 products with higher oxygen content than those previously reported were identified. High
46 molecular weight (HMW) products formed in the early stages of the oxidation have structures
47 consistent with aldol condensation products, peroxyhemiacetals, and esters. The size-dependent
48 distributions of HMW products in the SOA, as well as the effects of stabilized Criegee
49 intermediate (SCI) scavengers on HMW products and particle formation, confirm that HMW
50 products and reactions of Criegee intermediates play a crucial role in early stages of particle
51 formation. Our studies provide new insights into mechanisms of SOA formation and growth in
52 α -cedrene ozonolysis and the important role of sesquiterpenes in new particle formation as
53 suggested by field measurements.

54

55 **1. Introduction**

56 Organic aerosol is ubiquitous in the atmosphere and has an important influence on air quality
57 (Finlayson-Pitts and Pitts, 2000; Seinfeld and Pandis, 2006; Zhang et al., 2015), climate
58 (Kanakidou et al., 2005; IPCC, 2013), and human health (Mauderly and Chow, 2008; Shiraiwa et
59 al., 2012). Secondary organic aerosol (SOA) formed from the oxidation of volatile organic
60 compounds (VOCs) contributes a substantial fraction (up to 90%) of organic aerosol (Zhang et
61 al., 2007). Biogenic VOCs (BVOCs) such as isoprene (C_5H_8), monoterpenes ($C_{10}H_{16}$), and
62 sesquiterpenes ($C_{15}H_{24}$) account for ~ 90% of global VOC emissions (Guenther et al., 1995;
63 Goldstein and Galbally, 2007) and are the dominant contributors to global SOA formation upon
64 reaction with oxidants that are mainly anthropogenically derived (Kanakidou et al., 2005;
65 Hallquist et al., 2009).

66 Sesquiterpenes are an important class of BVOCs, with emissions being estimated as 9-29%
67 of those of monoterpenes (Helmig et al., 2007; Sakulyanontvittaya et al., 2008a). A variety of
68 sesquiterpenes have been detected in the atmosphere, including β -caryophyllene, α -humulene,
69 longifolene, α -farnesene, and α -cedrene (Helmig et al., 2007; Sakulyanontvittaya et al., 2008a;
70 Duhl et al., 2008; Bouvier-Brown et al., 2009). Sesquiterpenes have a high SOA forming
71 potential because of their large molecular sizes and, for many of them, the endocyclic double
72 bond structure which favors the formation of low-volatility oxidation products. The results of
73 laboratory chamber studies show high aerosol mass yields (defined as the mass of organic
74 aerosol formed per mass of precursor VOC reacted) from sesquiterpene oxidation (Hoffmann et
75 al., 1997; Lee et al., 2006; Ng et al., 2006; Winterhalter et al., 2009; Chen et al., 2012; Jaoui et
76 al., 2013; Yao et al., 2014; Tasoglou and Pandis, 2015). For example, an average 53% aerosol
77 mass yield was reported for ozonolysis and 55% for photooxidation (Jaoui et al., 2013). Field
78 and model studies have shown that sesquiterpene SOA comprises a significant fraction (6-32%)
79 of ambient organic aerosol from local to regional scales (Sakulyanontvittaya et al., 2008b; Hu et
80 al., 2008; Bouvier-Brown et al., 2009; Ding et al., 2014; Ying et al., 2015), with its contribution
81 comparable to that of monoterpene SOA in a variety of environments including rural, suburban,
82 and urban areas (Hu et al., 2008; Ding et al., 2014).

83 Although sesquiterpene oxidation contributes substantially to SOA, the underlying
84 mechanisms of SOA formation and growth are not well understood. Previous studies of

85 sesquiterpene oxidation have mainly focused on aerosol mass yields, the identities and formation
86 mechanisms of first-, second-, and higher-generation low molecular weight (LMW) oxidation
87 products, and their contributions to the formation of SOA (Hoffmann et al., 1997; Jaoui et al.,
88 2004, 2013; Lee et al., 2006; Ng et al., 2006; Kanawati et al., 2008; Reinnig et al., 2009;
89 Winterhalter et al., 2009; Li et al., 2011; Chan et al., 2011; Chen et al., 2012; Alfarra et al., 2012;
90 Yao et al., 2014). A few studies have suggested that sesquiterpenes play an important role in new
91 particle formation. For instance, field observations show that in new particle formation events,
92 sesquiterpene oxidation products significantly contribute to initial nucleation and growth (Boy et
93 al., 2008; Bonn et al., 2008). In addition, Bonn and Moortgat (2003) suggested that the
94 formation of oligomers was potentially important for nucleation. Lastly, laboratory studies of the
95 ozonolysis of β -caryophyllene and α -cedrene have reported a negative influence on particle
96 nucleation of species that can scavenge stabilized Criegee intermediate (SCI), supporting a key
97 role for sesquiterpene SCI in forming new particles (Bonn and Moortgat, 2003; Yao et al., 2014).

98 α -Cedrene (Fig.1) is found in air (Duhl et al., 2008), reacts rapidly with O₃ (Richters et al.,
99 2015), and is also an ideal compound for the study of sesquiterpene oxidation because (1) the
100 single C=C bond in its structure helps to simplify the oxidation chemistry and the product
101 distribution, and (2) its resemblance to other sesquiterpenes such as β -caryophyllene and α -
102 humulene in the endocyclic double bond structure (with a methyl group at one end) may enable,
103 to some degree, the generalization of SOA formation mechanisms for this class of compounds.
104 Previous studies of α -cedrene oxidation identified a number of products with molecular masses
105 below 300 Da in both the gas and particle phases, and proposed reaction mechanisms based on
106 known ozone chemistry (Jaoui et al., 2004, 2013; Reinnig et al., 2009; Yao et al., 2014).
107 Preliminary results from our lab (Zhao et al., 2015) subsequently identified higher molecular
108 weight products in the α -cedrene ozonolysis for the first time, and the SOA composition
109 suggested that the major mechanisms for particle formation are likely different than that for the
110 small alkenes (Sadezky et al., 2008; Zhao et al., 2015).

111 There have been very few measurements of the phase state of sesquiterpene SOA. The phase
112 state of SOA has an important influence on a number of physical and chemical processes of
113 aerosols, such as formation and growth (Koop et al., 2011; Perraud et al., 2012; Shiraiwa and
114 Seinfeld, 2012; Renbaum-Wolff et al., 2013), chemical aging (Renbaum and Smith, 2009;

115 Shiraiwa et al., 2011; Lignell et al., 2014; Chan et al., 2014; Slade and Knopf, 2014), and water
116 uptake (Mikhailov et al., 2009; Koop et al., 2011; Bones et al., 2012; Hodas et al., 2015;
117 Pajunoja et al., 2015), and thus affects their environmental and climate impacts. There is ample
118 evidence that in many cases, SOA may not be a low-viscosity liquid but rather a highly viscous
119 semi-solid (Virtanen et al., 2010; Cappa and Wilson, 2011; Koop et al., 2011; Vaden et al., 2011;
120 Saukko et al., 2012; Perraud et al., 2012; Abramson et al., 2013; Renbaum-Wolff et al., 2013;
121 Kidd et al., 2014a, b; Bateman et al., 2015). Recently, Saukko et al. (2012) and Pajunoja et al.
122 (2015) examined the phase state of SOA particles formed from OH and O₃ oxidation of
123 longifolene based on particle bounce measurements and found that longifolene SOA is solid or
124 semi-solid over a wide range of relative humidities. To better understand the phase state of
125 sesquiterpene SOA and its implications for various atmospheric processes, more particle phase
126 state measurements are needed.

127 In the present study, we report the results of a more comprehensive experimental
128 investigation of ozonolysis of α -cedrene. The phase state and mechanisms of growth of SOA are
129 examined by probing the evaporation of a tracer molecule, 2-ethylhexyl nitrate (2-EHN),
130 incorporated into the SOA during ozonolysis. The structures and formation mechanisms of high
131 molecular weight (HMW) products, as well as their roles in particle formation and growth, are
132 elucidated in light of their fragmentation mass spectra, accurate mass data, size-dependent SOA
133 composition, and the effects of water vapor and SCI scavenger. The identity and formation
134 mechanisms of some newly observed LMW (MW < 300 Da) oxidation products are also
135 explored.

136 **2. Experimental**

137 Experiments on α -cedrene ozonolysis were carried out both in a glass flow reactor and in static
138 Teflon chambers in the absence and presence of water vapor or SCI scavengers at 295 ± 1 K. No
139 seed particles or OH scavengers were used in any of these experiments. Table 1 and Figure S1
140 summarize the conditions and particle characteristics for various types of flow reactor and
141 chamber experiments.

142 **2.1 Flow reactor experiments**

143 The flow reactor (4.6 cm i.d. and 85 cm long) used in this study has been described in detail

144 previously (Zhao et al., 2015). α -Cedrene was added to the flow reactor by injecting the pure
145 liquid (Sigma-Aldrich and Extrasynthese, > 98%) into a flow of 1.76-2.96 L min⁻¹ of clean, dry
146 air (Praxair, ultra zero air) using an automated syringe pump (Pump Systems Inc., model NE-
147 1000). Ozone was generated by passing a flow of O₂ (Praxair, Ultra High Purity, 99.993%) at
148 0.24 L min⁻¹ through a pen-ray mercury lamp (model 11SC-2), and subsequently added to the
149 flow reactor downstream of the α -cedrene inlet. The O₃ concentration, determined using a UV-
150 VIS spectrometer (Ocean Optics, HR4000), was adjusted by changing the UV exposure of the O₂
151 via a movable metal cover surrounding the lamp. The total flow rate in the reactor was 2.0, 2.9,
152 or 3.2 L min⁻¹, corresponding to a residence time of 44, 30, or 27 s, respectively. Some of the
153 experiments were carried out in the presence of water vapor or formic acid, both of which can act
154 as SCI scavengers. Water vapor was added by bubbling a flow of clean air through nanopure
155 water (18.2 M Ω cm) into the flow reactor. The relative humidity of the airflow (~ 75% RH) in
156 the reactor was measured using a humidity probe (Vaisala, HMT234). Formic acid (Sigma-
157 Aldrich, \geq 95%) was added to the reactor using the same method as for α -cedrene.

158 The particle size distributions were measured at the outlet of the reactor using a scanning
159 mobility particle sizer (SMPS, TSI), which is equipped with an electrostatic classifier (model
160 3080), a long differential mobility analyzer (model 3081) and a condensation particle counter
161 (model 3776). When the size distribution of SOA was stable, the polydisperse particles were
162 collected onto a 47-mm PTFE filter (Millipore Fluoropore, 0.45 μ m pore size) at a flow rate of
163 1.9, 2.8, or 3.1 L min⁻¹, with venting of the remaining 0.1 L min⁻¹ aerosol flow to the hood. In
164 order to obtain sufficient particle mass for the analysis, the collection lasted 3-15 hours,
165 depending on the particle mass concentrations. Excellent collection efficiency (> 99%) was
166 obtained for particles of all diameters as established by SMPS measurements downstream of the
167 filter. The filter samples were extracted immediately with a 2-mL mixture (5:3 in v/v) of
168 methanol (OmniSolv, LC-MS grade) and hexanes (a mixture of hexane isomers, Fisher Scientific,
169 99.9%) under ultrasonication in an ice bath for 30 min. The extracts were then purged gently
170 using a flow of dry N₂ at room temperature to evaporate down to 1-mL. As hexanes are more
171 volatile than methanol, the remaining solvent in the extracts would be primarily methanol. The
172 resulting extracts were either analyzed directly using an LCT Premier electrospray ionization
173 time-of-flight mass spectrometer (ESI-ToF-MS, Waters) or diluted with water (OmniSolv, LC-
174 MS grade) to yield a final 50:50 water:methanol mixed solution, followed by analysis with a

175 Xevo TQS electrospray ionization triple quadrupole mass spectrometer (ESI-TQ-MS, Waters).
176 In order to verify that the sonication has no significant impact on SOA measurements, filter
177 extraction was performed instead, in some experiments, in the mixture of methanol/hexanes by
178 shaking for 30 min. No significant difference in product distribution was observed in ESI mass
179 spectra of the SOA extracted with and without sonication. In separate experiments, the chemical
180 composition of α -cedrene SOA was also measured in real time using direct analysis in real time
181 mass spectrometry (DART-MS).

182 **2.2 Chamber experiments**

183 Chamber experiments were carried out in 450 L Teflon chambers. Two types of α -cedrene
184 ozonolysis experiments were conducted: (i) under dry or humid (72% RH) conditions, and (ii) in
185 the absence or presence of gas phase 2-ethylhexyl nitrate (2-EHN), which was incorporated into
186 SOA during ozonolysis and used as a tracer molecule to probe the viscosity of SOA. The α -
187 cedrene was added using an automated syringe pump to inject a defined volume of pure liquid
188 into a flow of clean, dry air, which was directed into the chamber. Water vapor was added by
189 bubbling air through nanopure water into the chamber. 2-EHN (Sigma-Aldrich, 97%) was added
190 by injecting a known volume of liquid into the chamber. After 10 min to allow for mixing of the
191 gases (or two hours for the evaporation of the 2-EHN), ozonolysis was initiated by adding O₃
192 generated by a commercial ozone generator (Polymetrics, Model T-816) to the chamber.

193 For experiments CH1-CH3 (Table 1), SOA composition was examined online by a high
194 resolution time-of-flight aerosol mass spectrometer (HR-ToF-AMS, Aerodyne Research Inc.), or
195 by collection onto a PTFE filter at a flow rate of 12 L min⁻¹. Filter sampling started after 30 min
196 reaction time and lasted about 30 min. Because of the small volume of the chamber (450 L) and
197 relatively low SOA mass loading formed (see Table 1), in each experiment the SOA was sampled
198 onto one filter to ensure enough mass for ESI-MS analysis. The filter was extracted using the
199 same method as for SOA samples obtained in flow reactor experiments, followed by ESI-MS
200 analysis. For experiments CH4 and CH5, SOA formed without or with added 2-EHN at a 60 min
201 reaction time was collected onto a germanium (Ge) attenuated total reflectance (ATR) crystal
202 using a custom designed impactor (Kidd et al., 2014b) at a flow rate of 30 L min⁻¹. The SOA
203 impacted on the ATR crystal was subsequently probed using attenuated total reflectance-Fourier
204 transform infrared (ATR-FTIR) spectroscopy.

205 Most experiments were performed with excess O₃. In order to evaluate the influence of excess
206 O₃, which could lead to secondary oxidation of first generation products, some experiments were
207 performed with excess α -cedrene (Table 1, experiment CH3). The ESI mass spectra of SOA
208 formed in the presence of excess O₃ or excess α -cedrene are very similar, suggesting that the
209 excess O₃ has no observable influence on SOA formation. In addition, no significant difference
210 was observed in ESI mass spectra of SOA formed with or without added 2-EHN, suggesting that
211 the incorporation of 2-EHN into the SOA does not change its overall composition.

212 **2.3 SOA characterization**

213 In both flow reactor and chamber experiments, aerosol samples were directed through a 10-cm
214 monolith extruded carbon denuder (NovacarbTM; Mast Carbon, Ltd.) to remove the gas phase
215 species prior to particle collection on the filter. No significant difference in particle size
216 distribution was observed with or without the denuder. Blank experiments were also carried out
217 under the same experimental conditions as the ozonolysis experiments but without adding O₃ to
218 the flow reactor or the chamber.

219 **2.3.1 ATR-FTIR measurements**

220 The ATR crystal with impacted SOA was placed immediately into an ATR cell (volume ~ 2 cm³)
221 located in the sampling compartment of a Nicolet 6700 FTIR spectrometer (Thermo Scientific).
222 A flow of dry synthetic air at 100 mL min⁻¹ passed over the sample on the crystal. In some
223 experiments, this flow first passed through a pen-ray mercury lamp, producing 8 ppm O₃, in
224 order to probe the possibility of secondary oxidation of SOA components by O₃. Single beam
225 spectra at a resolution of 4 cm⁻¹ (128 scans) were collected before and after impaction of SOA.
226 The absorbance spectra of SOA on the crystal were derived from $\log_{10}(S_0/S_1)$ where S₀ and S₁
227 represent the single beam spectra of the clean and SOA-covered crystal, respectively. The IR
228 spectra of SOA were obtained over 20 hours of air or O₃ exposure to study the evolution and
229 evaporation of the impacted SOA during this period. In experiments performed in the presence
230 of 2-EHN, the signal at 1280 cm⁻¹ was followed over time to investigate the evaporation of 2-
231 EHN and determine its diffusion coefficient throughout the SOA matrix.

232 **2.3.2 ESI-MS measurements**

233 Extracts of both SOA and blank samples were analyzed by ESI-ToF-MS operated in either

234 positive or negative ion mode. The operating conditions of this mass spectrometer were
235 described previously (Zhao et al., 2015). Mass spectra were acquired in the 200-1000 Da mass
236 range. Although ESI often forms multiply charged ions, the major ions observed throughout the
237 mass spectra are in the singly charged state, as indicated by the unity spacing of the isotope
238 peaks (Greaves and Roboz, 2013). Sodium adducts $[M+Na]^+$ were the primary ions observed in
239 the positive ion mode (ESI+) and deprotonated ions $[M-H]^-$ in the negative ion mode (ESI-).
240 Mass spectra of blanks, in which the peaks are mainly attributed to the impurities in the solvent
241 and filter and have intensities of 10-30% of SOA peaks, were subtracted from those of SOA
242 samples. Accurate mass measurements were performed using sodium formate, polyethylene
243 glycol, and polyethylene glycol monomethyl ether as mass calibration standards. In addition,
244 SOA extracts were analyzed using ESI-TQ-MS to record the fragmentation spectra (MS^2) of
245 selected ions, from which typical structures of reasonable products based on likely mechanisms
246 were tentatively assigned. The parent ions selected by the first quadrupole (Q1) enter the
247 collision cell (Q2), where they fragment via collision-induced dissociation (CID) with argon as
248 the collision gas at collision energies of 20-30 eV, and the resulting fragment ions are monitored
249 by the third quadrupole (Q3). In this case, the ESI source was operated in positive ion mode
250 under optimized conditions as follows: capillary voltage 3.2 kV, desolvation gas flow 1000 L h⁻¹,
251 desolvation gas temperature 500 °C, nebulizer gas pressure 7 bar.

252 **2.3.3 AMS measurements**

253 An Aerodyne HR-ToF-AMS was used to analyze the chemical composition and to examine O:C
254 ratios of polydisperse SOA formed in the chamber. Due to the small sizes of the SOA formed in
255 the flow reactor, it was impossible to measure them with the AMS, and thus all AMS results
256 presented hereafter are exclusively from the chamber studies. A detailed description of this
257 instrument has been given elsewhere (DeCarlo et al., 2006). The SOA sampled into the
258 instrument was vaporized at 600 °C. High resolution MS data were collected in both V-mode and
259 W-mode and analyzed using the “Improved-Ambient” method (Canagaratna et al., 2015).
260 Measurements with a particle filter were carried out before each experiment to aid in
261 quantification of the CHO⁺ fragment at m/z 29 which has interference from gaseous ¹⁵NN and
262 can significantly affect elemental analysis.

263 **2.3.4 DART-MS measurements**

264 Direct analysis in real time mass spectrometry (DART-MS) is an atmospheric pressure soft
265 ionization method used to examine chemical composition of solid and liquid samples after
266 thermal desorption. A more detailed description of this mass spectrometric technique is given
267 elsewhere (Cody et al., 2005; Nah et al., 2013). In this work, α -cedrene SOA formed in the flow
268 reactor under dry conditions was measured in real time using a Xevo TQS triple quadrupole mass
269 spectrometer (Waters) equipped with a commercial DART ion source (IonSense, DART SVP
270 with Vapur[®] Interface). As DART-MS is a surface-sensitive technique, to ensure that the bulk of
271 particles can be effectively probed, the aerosol stream exiting the flow reactor, in which the gas
272 phase species was removed using a denuder, was heated to 160 °C before entering into the
273 ionization region. The DART ion source was operated in either positive or negative ion modes
274 with He as the reagent gas under the following conditions: He gas flow 3.1 L min⁻¹; He gas
275 temperature 200 °C; grid electrode voltage 350 V. The configuration of the DART ion source
276 interfaced to the MS is shown in Fig. S2.

277 **3. Results and discussion**

278 **3.1 ATR-FTIR measurements**

279 Figure 2a is a typical ATR-FTIR spectrum recorded immediately following impaction of α -
280 cedrene SOA formed in the chamber in the absence of 2-EHN. The strong C=O band at 1706
281 cm⁻¹ suggests that aldehydes/ketones are important SOA components. A shoulder at 1762 cm⁻¹
282 may indicate the presence of carboxylic acids, esters, or other C=O group-containing species
283 with a more electronegative atom such as oxygen being attached to the carbonyl carbon (Socrates,
284 2001; Kidd et al., 2014a).

285 Figure 2b is a difference spectrum showing the changes in SOA after exposure to a flow of
286 clean dry air for 20 hours. The positive and negative peaks in the spectrum represent an increase
287 or decrease respectively in the functional groups in SOA due to air exposure. There is a decrease
288 in peaks at 3416, 1762, 1371 and 1076 cm⁻¹ and an increase in peaks at 1735, 1706, 1410 and in
289 the 1100-1350 cm⁻¹ region. Note that there is no obvious change in the C-H peaks around 2957
290 cm⁻¹, suggesting that evaporation of organic species from SOA during air exposure is not
291 important. Therefore, the changes in SOA as indicated by the difference spectra are due to
292 chemistry occurring in SOA during air exposure. One of the possible processes is the

293 decomposition of oligomers that comprise a significant fraction of α -cedrene SOA as discussed
294 later. For example, decomposition of peroxyhemiacetals and aldol condensation products to their
295 precursors can lead to the loss of O-H groups and concomitant formation of ketone/aldehyde
296 C=O groups. The decomposition of oligomers in SOA was supported by ESI-MS measurements
297 of SOA collected on Teflon filters and then exposed to a flow of clean dry air; thus the relative
298 ion intensity of oligomers to LMW products in the mass spectrum of SOA extracted after 20
299 hours of air exposure is $\sim 15\%$ lower compared to that of SOA extracted immediately following
300 collection. The difference spectrum of the SOA film exposed to clean humid air at 89% RH for
301 40 min (Fig. S3) shows a broad band centered at 3426 cm^{-1} and a narrow band at 1640 cm^{-1}
302 resulting from the stretching and bending vibration of adsorbed water respectively, with relative
303 strength of stretching vs. bending of ~ 2 . The absence of a negative peak at 1640 cm^{-1} in the
304 difference spectrum after dry air exposure as shown in Fig. 2b, therefore, suggests that the
305 contribution of water to the loss in the O-H band at 3416 cm^{-1} is minor and the decrease in this
306 region must be due to a change in SOA components.

307 Figure 2c shows the difference spectrum of SOA upon exposure to 8 ppm O_3 for 20 hours
308 which is very similar to the difference spectrum of SOA after 20 hours of clean air exposure (Fig.
309 2b). This shows that the α -cedrene SOA oxidation products are not reactive toward O_3 , at least
310 as detectable by changes in the infrared spectrum.

311 **3.2 Viscosity and phase state of SOA**

312 In order to probe the phase state of α -cedrene SOA, a relatively volatile organic species, 2-
313 ethylhexyl nitrate (2-EHN, $P_{\text{sat}} = 1.4 \times 10^{-4}$ atm at 295 K, Pankow and Asher, 2008), was
314 included in one type of experiment (CH-5, Table 1) so that it could be incorporated into the SOA
315 as it is formed in the chamber. The evaporation of 2-EHN from the SOA impacted onto the ATR
316 crystal upon exposure to a flow of clean dry air was followed with time to probe the phase state
317 of SOA.

318 Figure 3a shows a digital photograph of a typical impaction pattern on the ATR crystal of α -
319 cedrene SOA formed in the chamber in the presence of gas phase 2-EHN. The SOA impacts and
320 adheres to the crystal, forming a narrow film ~ 1.0 mm in width at the centerline. Similar
321 impaction patterns were also observed for the SOA formed without added 2-EHN. Figure 3b

322 shows the SOA number and mass size distributions after 60 min reaction time in the chamber, as
323 well as the collection efficiency of the impactor as a function of particle diameter (Kidd et al.,
324 2014b). By dividing the particles into a number of 10-nm size bins and applying the average
325 particle collection efficiency at each bin, the SOA mass collected on the crystal is estimated to be
326 42 μg using $\sum m_i f_i$, where m_i and f_i are the particle mass and average particle collection efficiency
327 at each size bin, respectively. Since the particle wall loss in the chamber during impaction was
328 not considered, this mass should be an upper limit. Assuming a particle density of 1.1 g cm^{-3}
329 (Yao et al., 2014), the maximum average thickness of the SOA film on the ATR crystal is
330 estimated to be $L = 0.54 \mu\text{m}$. This estimate of L relies on the assumption that SOA impacted on
331 the crystal forms a uniform narrow film. This may underestimate the film thickness by as much
332 as a factor of two if, rather than forming a thin film, the SOA is collected in separate columns
333 immediately below the impactor holes. An additional, smaller, uncertainty in L results from
334 variation in the collection efficiency of the impactor over the particle size range of interest (see
335 Fig. 3b). We estimate the combination of these two to give an uncertainty in L of about a factor
336 of two.

337 The refractive index of α -cedrene SOA is not known but a value of ~ 1.5 is reasonable based
338 on literature values for SOA from other biogenic organic oxidations (Lambe et al., 2013; Kim et
339 al., 2014). The penetration depth of the IR beam at 1280 and 1635 cm^{-1} , peaks which correspond
340 to the absorption bands of organic nitrate as discussed below, is then calculated to be 0.52 and
341 $0.41 \mu\text{m}$ (Harrick, 1967), respectively, for SOA on a Ge crystal. This suggests that the entire
342 depth of the SOA film on the ATR crystal can be probed reasonably well by the IR beam in the
343 region of interest.

344 Figure 4a is a typical ATR-FTIR spectrum of α -cedrene SOA formed in the presence of 2-
345 EHN in the chamber under dry conditions. The spectrum is essentially the same as that of SOA
346 formed without 2-EHN (Fig. 2a) except that there are two new bands at 1635 and 1280 cm^{-1}
347 resulting from the vibrations of nitrate (Socrates, 2001; Bruns et al., 2010; Perraud et al., 2012)
348 when 2-EHN is present. Figure 4b shows the difference spectrum of SOA after exposure to a
349 flow of clean dry air for 20 hours. In addition to the spectral features similar to the difference
350 spectrum of 2-EHN-free SOA (Fig. 2b), there is a small loss of nitrate peaks at 1635 cm^{-1} and
351 1280 cm^{-1} , indicating some evaporation of 2-EHN from SOA during air exposure. Figure 5

352 shows the temporal evolution of the integrated area of the nitrate peak at 1280 cm^{-1} over 20
353 hours of air exposure. It can be seen that after 20 hours of air exposure, only $\sim 27\%$ of 2-EHN
354 evaporated from the SOA. This slow evaporation indicates that 2-EHN is incorporated in the
355 bulk of the SOA, and that the SOA must be a high-viscosity semi-solid rather than a liquid where
356 diffusion would be much more rapid (Shiraiwa et al., 2011; Koop et al., 2011).

357 The incorporation of high-volatility 2-EHN into the bulk of high-viscosity SOA is consistent
358 with a condensation particle growth mechanism (Finlayson-Pitts and Pitts, 2000; Seinfeld and
359 Pandis, 2006; Riipinen et al., 2011; Perraud et al., 2012), for which organic species condense
360 kinetically onto the surface of pre-existing particles and become buried and incorporated into the
361 bulk by incoming low volatility organics. It is important to note that in the ATR-FTIR spectrum
362 (Fig. 4c) of α -cedrene SOA formed without added 2-EHN in the chamber and then exposed to 20
363 ppm 2-EHN in the ATR cell for one hour, the absorption bands associated with organic nitrate at
364 1635 and 1280 cm^{-1} are negligible. This observation suggests that the uptake of 2-EHN into or
365 onto previously formed SOA is not important.

366 Assuming that the evaporation of 2-EHN is determined only by its diffusion in the film of
367 SOA impacted on the ATR crystal and that the diffusion follows Fick's Law, for a film with
368 uniform 2-EHN concentration (C_0) at $t = 0$ and zero concentration at the surface for $t > 0$, the
369 total fraction (F) of 2-EHN remaining in the film at time t can be expressed as (Crank, 1975;
370 Mehrer, 2007)

$$F = \frac{8}{\pi^2} \sum_{j=0}^{\infty} \frac{1}{(2j+1)^2} \exp\left[-\frac{(2j+1)^2 \pi^2 Dt}{4L^2}\right] \quad j = 0, 1, 2, \dots \quad (1)$$

371 In eq. (1), D is the diffusion coefficient of 2-EHN in the SOA and L is the thickness of the SOA
372 film on the ATR crystal. A best fit of the evaporation data of 2-EHN in Fig. 5 to eq. (1) gives
373 $D/L^2 = 5.6 \times 10^{-5}\text{ min}^{-1}$. With the SOA film thickness L of $0.54\text{ }\mu\text{m}$ estimated above, the
374 diffusion coefficient (D) of 2-EHN in SOA is calculated to be $3 \times 10^{-15}\text{ cm}^2\text{ s}^{-1}$, consistent with
375 the D values of the order of $\sim 10^{-15}\text{ cm}^2\text{ s}^{-1}$ predicted from the time scale for evaporation
376 combined with the estimated thickness of the SOA layer (Shiraiwa et al., 2011; Koop et al.,
377 2011). The uncertainty in L of about a factor of two described above translates into an
378 uncertainty in D of about a factor of four. However, this value for D is within the range of

379 diffusion coefficients that would be expected in a highly viscous semi-solid matrix, i.e., $D = 10^{-10}$
380 $-10^{-20} \text{ cm}^2 \text{ s}^{-1}$ (Shiraiwa et al., 2011; Koop et al., 2011), confirming that α -cedrene SOA is a high-
381 viscosity semi-solid. However, because of their small sizes, these particles do not have enough
382 momentum to bounce as they impact on the ATR crystal, as seen for larger SOA from α -pinene
383 oxidation in earlier studies (Kidd et al., 2014a, b). Recently, Saukko et al. (2012) and Pajunoja et
384 al. (2015) reported the formation of semi-solid SOA from the oxidation of the sesquiterpene
385 longifolene based on particle bounce measurements. However, to our knowledge, the present
386 work shows the first measurement of the diffusion coefficient of an organic species in
387 sesquiterpene SOA.

388 **3.3 SOA composition**

389 Figure 6 shows typical ESI+ and ESI- mass spectra of SOA formed from α -cedrene ozonolysis
390 in the flow reactor at 30 s reaction time. Ions in the mass range m/z 220-350 correspond to low
391 molecular weight (LMW) products derived directly from oxidation of α -cedrene and retaining
392 much of the structure of the parent compound (hereafter termed P1 products). Those with m/z >
393 420 correspond to high molecular weight (HMW) products formed using two, three, or four P1
394 products (hereafter termed P2, P3, and P4 products, respectively) as building blocks. We try to
395 avoid using the terms "dimer", "trimer", etc. which may imply simple combinations of smaller
396 species whereas P2, P3, etc. are clearly complex combinations of different LMW products. As
397 discussed above, there is no evidence that any of these peaks arise from multiple charging of
398 higher molecular weight species. The data presented in Fig. 6 suggest that P1 and P2 products
399 comprise a dominant fraction of α -cedrene SOA. Compared to the ESI+ spectrum, the
400 corresponding ions in the ESI- spectrum are generally 24 Da lower in mass. This is consistent
401 with the fact that the ions observed in the ESI+ mode are primarily sodium adducts while those
402 in the ESI- mode are deprotonated ions with a predominant contribution from carboxylic acids.

403 Figure 7 shows the ESI mass spectra of polydisperse α -cedrene SOA (size distributions are
404 given in Fig. S1a) with geometric mean diameters of 15 and 23 nm formed in the flow reactor at
405 the same concentrations of α -cedrene and O_3 but different reaction times (27 s and 44 s) under
406 dry conditions (Table 1, experiments FR1-FR2). Among P2 products, those at m/z 481-543 are
407 the most abundant ones in the flow reactor SOA and they have a greater contribution to the
408 smaller particles formed at shorter reaction times (Fig. 7a). Conversely, P1 products contribute

409 more to larger particles formed at longer reaction times (Fig. 7b). Figure S4 shows additional
410 ESI mass spectra of polydisperse α -cedrene SOA particles of different geometric mean diameters
411 (13, 18, and 26 nm) formed in the flow reactor at the same reaction time (30 s) but different
412 concentrations of α -cedrene under dry conditions (Table 1, experiments FR3-FR5). A similar
413 size-dependent distribution of P1 and P2 products is observed. These results suggest that P2
414 products at m/z 481-543 may play an important role in initial particle formation, while P1
415 products contribute significantly to particle growth.

416 Figure 8 shows typical ESI⁺ and ESI⁻ mass spectra of α -cedrene SOA formed in the
417 chamber. The chamber SOA has a geometric mean diameter of 66 nm, larger than those formed
418 in the flow reactor (13-26 nm, depending on the experimental conditions) due to the longer
419 reaction times and hence greater extents of reaction. Figure 8 shows that the chamber particles
420 also have relatively more P1 products, in agreement with the important role of P1 products in
421 particle growth. In addition, the subset of P2 products with $m/z > 543$ in the positive ion mode
422 account for a greater fraction of total P2 products in the chamber SOA than in the flow reactor
423 SOA (Figs. 6a and 7). This suggests that these larger P2 products (i.e., $m/z > 543$) are mainly
424 formed at longer reaction times in the chamber and contribute mainly to particle growth.

425 It is known that P1 products may undergo ion-molecule reactions to form noncovalently
426 bound clusters in the ESI source (Muller et al., 2009; Gao et al., 2010), and the formation of such
427 clusters, if it occurs, is expected to be positively correlated with the abundance of P1 products.
428 However, as shown in Figs. 7 and S4, the signal intensity ratio of P2 to P1 products is inversely
429 dependent on the size of SOA. This suggests that the P2 products observed in ESI mass spectra
430 are unlikely to be artifacts of in-source clustering. In addition, HMW products in α -cedrene SOA
431 are also detected in real time by DART-MS that employs a different ionization method. Figure
432 S5 shows typical DART⁺ (positive ion mode) and DART⁻ (negative ion mode) mass spectra of
433 flow reactor α -cedrene SOA, which was heated to 160 °C before introduction into the ionization
434 region. The masses of P1 and P2 products in the DART⁺ mass spectrum are generally 22-24 Da
435 lower than those in the ESI⁺ mass spectrum (Fig. 6), consistent with the ions detected by DART-
436 MS in the positive mode being primarily $[M+H]^+$, M^+ , and $[M-H]^+$ (Cody et al., 2005; Nah et al.,
437 2013). In contrast, essentially the same masses for P1 and P2 products were observed in DART⁻
438 and ESI⁻ mass spectra, in both of which the ions are predominantly $[M-H]^-$. There are some

439 differences between ESI and DART mass spectra that are likely due to the heating of incoming
440 aerosol stream for DART-MS and the higher DART source temperature. Overall, DART-MS
441 measurements further support that the P2 products observed by ESI-MS are not artifacts from the
442 ion source.

443 Previous studies have reported an OH yield of 62-67% from ozonolysis of α -cedrene (Shu
444 and Atkinson, 1994; Yao et al., 2014). Therefore, reaction with OH could play a role in α -
445 cedrene oxidation in the absence of an OH scavenger. We reported in a previous study (Zhao et
446 al., 2015) ESI-MS spectra in the absence and presence of cyclohexane, which showed that the
447 relative intensity of P2-P4 peaks in the presence of cyclohexane is smaller. This suggests that
448 OH oxidation may contribute to the formation of HMW species.

449 Possible structures and formation mechanisms of typical P1 and P2 products (as labeled in
450 Fig. 6) were explored based on their fragmentation mass spectra (MS^2), accurate mass data,
451 previously identified P1 products (Jaoui et al., 2004, 2013; Reinnig et al., 2009; Yao et al., 2014),
452 and likely reaction mechanisms of terpene ozonolysis. To the best of our knowledge, this is the
453 first detailed examination of HMW products initially reported (Zhao et al., 2015) in this system.

454 **3.3.1 P1 products.**

455 The characterization of the molecular structures and formation mechanisms of P1 products from
456 the ozonolysis of α -cedrene has been the emphasis of earlier studies (Jaoui et al., 2004, 2013;
457 Reinnig et al., 2009; Yao et al., 2014). A number of multifunctional P1 products were tentatively
458 identified using different mass spectrometric and derivatization techniques in those studies.
459 Figure S6 shows the ESI(+)- MS^2 spectra as well as the proposed structures of the products with
460 m/z values in the range of 245-291 Da measured in the current experiments. As reported by
461 Tolocka et al. (2004), fragmentation of sodium adducts is difficult so the product ion intensities
462 are relatively weak. However, fragmentation is seen to occur mainly via loss of 18 Da (H_2O ,
463 indicating the presence of an aldehyde, carboxylic or hydroxyl group), loss of 30 Da (CH_2O ,
464 indicating the presence of a formyl group), loss of 32 Da (CH_4O , indicating the presence of a
465 hydroxymethyl group), loss of 44 Da (CO_2 or C_2H_4O , indicating a carboxylic or acetyl group),
466 and loss of 46 Da (CH_2O_2 , indicating a carboxylic group). The fragmentation pathways of the
467 functional groups as shown here generally agree with those reported in the literature (Tolocka et

468 al., 2004; Hall and Johnston, 2012), where ESI-MS in positive ion mode was used to characterize
469 the structure of reaction products from ozonolysis of α -pinene. The structures assigned to the
470 products at m/z 245-291 are consistent with those reported in the previous studies (Jaoui et al.,
471 2004, 2013; Reinnig et al., 2009; Yao et al., 2014). In many cases, the MS² spectra can be due to
472 multiple isomeric structures. Table 2 shows accurate mass data for these P1 products. Their
473 measured accurate masses are for the most part in excellent agreement with the elemental
474 formulae for their proposed structures, the exception being P1-289 in the negative ion mode.

475 In addition to the products reported previously (Jaoui et al., 2004, 2013; Reinnig et al., 2009;
476 Yao et al., 2014), some products corresponding to the $[M+Na]^+$ at m/z 305-323 not previously
477 identified were detected by ESI-MS. Figure S7 shows the parent ion spectra of these sodiated
478 ions at collision gas energy (CE) of 6 eV that is equivalent to the CE for MS scan. Parent ion
479 spectra of m/z 305-323 have negligible parents but strong signals from themselves at this low CE.
480 This strongly suggests that these ions are molecular ions rather than fragments from larger
481 products. However, as shown in the insets of Fig. S7, significant parents are observed for these
482 ions when the CE is increased to 20 eV. This is reasonable since these P1 products can be
483 precursors of HMW products, which is expected to fragment readily back to its precursors at
484 higher CEs, and that the fragmentation of HMW products formed from other P1 products is also
485 likely to give fragments with m/z values of 305-323. These P1 products were also observed by
486 DART-MS in the m/z 281-301 region primarily as $[M+H]^+$ with some contribution from $[M]^+$ in
487 the positive ion mode, or $[M-H]^-$ ions in the negative ion mode (Fig. S5), consistent with DART-
488 MS studies of single compounds (Nah et al., 2013).

489 Figure 9 shows the potential structures of these newly observed P1 products proposed based
490 on their ESI-MS² spectra (Fig. S8). The fragments resulting from the loss of water and multiple
491 oxygenated functional groups such as carboxylic, carbonyl, and hydroxyl groups were observed.
492 It was found in our previous study that the formation of the products corresponding to m/z 305-
493 323 ions continues in the presence of cyclohexane as an OH scavenger (Zhao et al., 2015). This
494 suggests that the newly observed products are not formed by OH oxidation, but rather by O₃
495 oxidation. Figure S9 illustrates some potential formation mechanisms for these newly observed
496 products. The Criegee intermediates (CIs) form peroxy (RO₂) radicals via the vinyl
497 hydroperoxide (VHP) channel. The conversion of RO₂ to alkoxy (RO) radicals and the

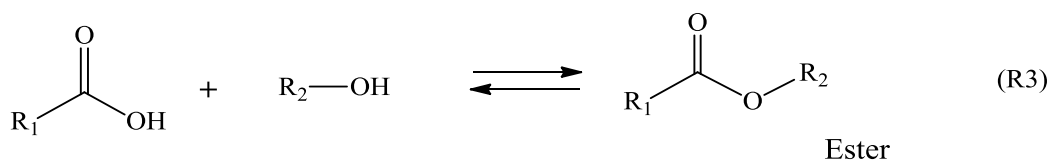
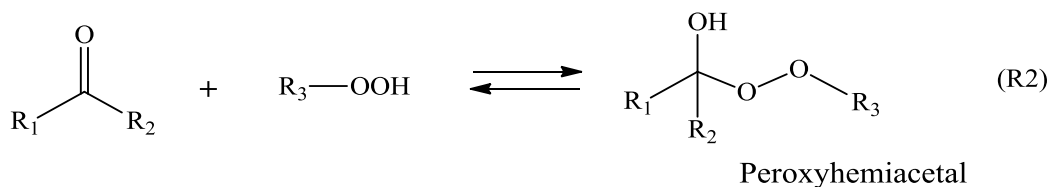
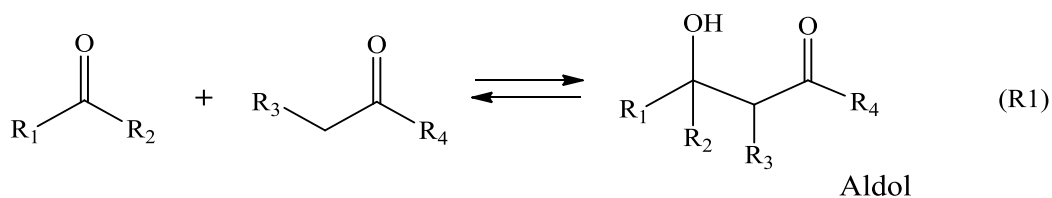
498 subsequent intramolecular H-abstraction/O₂ addition lead again to RO₂ radicals, which can
499 further undergo similar reactions to form RO₂ radicals with higher oxygen content. Termination
500 reactions with RO₂ or HO₂ radicals lead to the formation of the newly observed products.

501 While accurate mass data of these products (Table 2) agree well with the proposed structures,
502 there may be additional structures and reaction pathways in the formation of the P1 products at
503 *m/z* 305-323 via the VHP channel of CIs that contribute to these peaks. For example, because of
504 their large carbon skeleton, RO radicals may have multiple isomerization pathways to form
505 different structures with the same elemental composition.

506 Secondary ozonides formed through intramolecular reactions of SCI were observed as the
507 major gas phase products from ozonolysis of α -cedrene (Yao et al., 2014) and β -caryophyllene
508 (Winterhalter et al., 2009), with their formation being significantly suppressed by the addition of
509 water vapor. In the present study, although a sodiated ion with *m/z* 275 and elemental
510 composition of C₁₅H₂₄O₃Na, consistent with the mass and formula of the intramolecularly
511 formed SOZ, was observed in ESI (+) mass spectra of α -cedrene SOA, as will be discussed in
512 Sect. 3.4, the relative intensity of this ion in the mass spectra does not decrease at all at 75% RH
513 and is still pronounced with high concentrations of formic acid (15 ppm) added as an SCI
514 scavenger. This indicates that the ion at *m/z* 275 is unlikely to be the SOZ. Similarly, Yao et al.
515 (2014) did not observe the SOZ in the particle phase using HPLC-MS and GC-MS. A possible
516 explanation is that the intramolecularly formed SOZ has a relatively high vapor pressure ($1.2 \times$
517 10^{-6} atm at 295 K) and therefore a low potential to partition to the particle phase.

518 **3.3.2 P2 products.**

519 Table 2 gives the accurate masses and elemental formulae of the most abundant P2 products as
520 labeled in the ESI mass spectra (Fig. 6a). Figure 10 shows the proposed potential structures of
521 these products based on their accurate mass data and ESI-MS² spectra (Fig. S10) (see
522 Supplement for the detailed discussion). These structures include aldol condensation products
523 (formed from the reaction of two carbonyl compounds, Reaction R1), peroxyhemiacetals
524 (formed from the reaction of a carbonyl compound and an organic hydroperoxide, Reaction R2),
525 and esters (formed from the reaction of a carboxylic acid with an alcohol, Reaction R3), with the
526 building blocks being the P1 products typically observed in the SOA.



527

528 Aldol condensation products and peroxyhemiacetals are the most commonly identified
 529 structures. Of 17 proposed structures for these P2 products, ten are aldol condensation products
 530 and five are peroxyhemiacetals. Except for products P2-481 and P2-497 that are identified as
 531 aldol condensation products, other P2 products may have contributions from multiple structures.
 532 For example, product P2-511 may have contributions from both aldol condensation products and
 533 esters, and products P2-513, P2-527, and P2-543 may have contributions from both aldol
 534 condensation products and peroxyhemiacetals. Although no detailed data concerning the
 535 formation of such HMW products during sesquiterpene ozonolysis are available in the literature,
 536 a number of laboratory and field studies have found that aldol condensation products,
 537 peroxyhemiacetals, and esters are the major HMW products detected in the SOA formed from
 538 ozonolysis of monoterpenes (e.g., α -pinene and β -pinene) (Hoffmann et al., 1998; Tolocka et al.,
 539 2004; Docherty et al., 2005; Muller et al., 2008, 2009; Heaton et al., 2009; Gao et al., 2010;
 540 Yasmeeen et al., 2010; Hall and Johnston, 2012; Kristensen et al., 2013, 2014; Witkowski and
 541 Gierczak, 2014; X. Zhang et al., 2015). Formation of such products has traditionally been
 542 thought to occur via acid-catalyzed reactions (reactions R1-R3) in the condensed phase (Kroll
 543 and Seinfeld, 2008; Hallquist et al., 2009; Yasmeeen et al., 2010; Ziemann and Atkinson, 2012),
 544 although some recent studies suggested that such a process is not favored for esterification in
 545 SOA (Birdsall et al., 2013; DePalma et al., 2013; Kristensen et al., 2014; X. Zhang et al., 2015).
 546 Formation of peroxyhemiacetals has also been suggested to be thermodynamically favorable in

547 the gas phase (DePalma et al., 2013), although whether the kinetics are sufficiently fast is not
548 known. It is noted that there may be some decomposition of HMW products over time, for
549 example, over 20 hours of clean air exposure as discussed earlier.

550 **3.4 The effects of water vapor and SCI scavenger**

551 The reaction of α -cedrene with ozone has a very high SCI yield (> 88%) (Yao et al., 2014). If
552 SCI reactions are key to SOA formation in this system, the addition of SCI scavengers such as
553 water vapor and formic acid should have significant influence on the formation of SOA.

554 Figure 11 shows the size distributions of SOA formed from ozonolysis of α -cedrene in the
555 flow reactor under dry conditions, at 75% RH, or in the presence of 15 ppm formic acid. SOA
556 with very similar number concentrations is formed with or without added water vapor, while
557 significantly fewer, but larger, particles are formed in the presence of formic acid. Recent
558 kinetics measurements of the CH₂OO CI reaction with water vapor (monomer and dimer) give
559 rate constants of $k_{dimer} = (4.0 - 6.5) \times 10^{-12} \text{ cm}^3 \text{ molecule}^{-1} \text{ s}^{-1}$ (Chao et al., 2015; Lewis et al.,
560 2015) and $k_{monomer} = 3.2 \times 10^{-16} \text{ cm}^3 \text{ molecule}^{-1} \text{ s}^{-1}$ (Berndt et al., 2015). The rate constant for the
561 reaction of CH₂OO with formic acid is much larger, $k_{HCOOH} = 1 \times 10^{-10} \text{ cm}^3 \text{ molecule}^{-1} \text{ s}^{-1}$ (Welz
562 et al., 2014). The reactivity of Criegee intermediates has been shown to depend on structure for
563 a number of reasons, including different extents of pressure stabilization of excited CI, different
564 reactivities for the *syn*- and *anti*- forms, and different natures of the groups attached to the central
565 CI carbon (Ryzhkov and Ariya, 2004; Anglada et al., 2011; Donahue et al., 2011; Vereecken et al.,
566 2012; Taatjes et al., 2013; Welz et al., 2014). While the α -cedrene CI is clearly very different
567 than CH₂OO, if the rate constants for the latter are representative in a relative sense, the ratio of
568 the rates for reaction of the α -cedrene CI with formic acid and water dimer relative to water
569 monomer are ~ 240: 18: 1 under our experimental conditions ($3.7 \times 10^{14} \text{ HCOOH cm}^{-3}$, $4.8 \times$
570 $10^{17} \text{ H}_2\text{O cm}^{-3}$ and $5.1 \times 10^{14} (\text{H}_2\text{O})_2 \text{ cm}^{-3}$, based on a water equilibrium constant of 0.0536 atm^{-1}
571 (Ruscic, 2013)). Thus, it is not surprising that formic acid has a much greater impact than water.
572 Furthermore, the large effects of formic acid further support the importance of the α -cedrene CI
573 in SOA formation. These impacts of water and formic acid are in agreement with those reported
574 by Yao et al. (2014) who reported a similar quenching effect of added acetic acid on particle
575 formation in the α -cedrene ozonolysis, but relatively little impact of water vapor.

576 Figures 12a and 12b show the ESI mass spectra of α -cedrene SOA formed in the flow reactor
577 without and with added water vapor, respectively. There are no significant differences in product
578 distribution with and without added water vapor. In addition, ESI-MS² measurements show that
579 typical P1 and P2 products as labeled in both mass spectra have very similar MS² spectra,
580 suggesting that the product composition is not impacted by the presence of water. Measurements
581 of the chamber SOA by AMS (see Fig. S11) also did not show significant differences in the
582 particle mass spectra upon water addition. On the other hand, Figure 12c shows the ESI mass
583 spectra of SOA formed in the presence of 15 ppm formic acid. The formation of HMW products
584 is significantly reduced as are the number of peaks in the P1 product region. However, P1
585 products at m/z 259, 275, and 291, as well as P2 products, for example, at m/z 527, 543, and 559,
586 are still evident. All of these P1 products have very similar MS² spectra (and thus likely similar
587 structures) to those formed in the absence of formic acid. In contrast, P2 products at m/z 527 and
588 543 show significantly different MS² spectra compared to those obtained without added formic
589 acid.

590 Yao et al. (2014) reported an increase in the formation of α -cedronaldehyde in the presence of
591 acetic acid, consistent with an increase in the present studies in the relative abundance of the P1
592 product at m/z 259 assigned to α -cedronaldehyde when formic acid was added (Fig. 12c). The
593 reaction of α -cedrene SCI with formic acid is expected to form α -formyloxy hydroperoxide (MW
594 298 Da), which is believed to contribute to SOA growth. While the corresponding sodium
595 adduct at m/z 321 is not observed in the mass spectrum, this is not surprising as hydroperoxides
596 are likely to undergo decomposition during SOA sampling and analysis (Witkowski and
597 Gierczak, 2013).

598 Comparison of Fig. 12c to Fig.12a shows that HMW products (P2-P4) formed with added
599 formic acid are less important than those produced in the absence of formic acid. Combined
600 with the smaller number concentration (Fig. 11), the data suggest that HMW products must be
601 important in new particle formation. As fewer particles are formed with the addition of formic
602 acid, more P1 products are available for each particle to grow to larger sizes.

603 **3.5 Mechanisms**

604 The size-dependent composition of α -cedrene SOA and the effect of SCI scavengers on particle

605 formation suggest that HMW products (P2-P4) play an important role in the initial stages of
606 particle formation. This is consistent with earlier suggestions in simpler systems that higher
607 molecular weight products of alkene ozonolysis are primarily responsible for nucleation, while
608 many different products from low to high molecular weight can contribute to growth (Lee and
609 Kamens, 2005; Sadezky et al., 2008; Winkler et al., 2012; Zhao et al., 2013; Ehn et al., 2014;
610 Kidd et al., 2014a; Zhao et al., 2015; X. Zhang et al., 2015). Bonn and Moortgat (2003)
611 estimated an upper limit for the saturated vapor pressure (P_{sat}) of nucleating species produced
612 from sesquiterpene ozonolysis to be 1.2×10^{-13} atm. Donahue et al. (2013) also suggested that
613 organic vapors with $P_{\text{sat}} < 10^{-13}$ atm may contribute to particle nucleation. The P_{sat} of typical P1
614 products, as well as the P2 products (e.g., ester and peroxyhemiacetal) are estimated by
615 averaging the predictions (see Table S1) from two group contribution methods, SIMPOL.1
616 (Pankow and Asher, 2008) and EVAPORATION (Compernelle et al., 2011), and are shown in
617 Figure 13. The P_{sat} for the P2 products are 3-6 orders of magnitude lower than the suggested
618 nucleation threshold, consistent with their important contributions to initial particle formation.
619 The newly observed products (P1-321 and P1-323) also have vapor pressures lower than the
620 nucleation threshold and thus may in principle also contribute to nucleation. This is also
621 expected to be the case for the HMW P3 and P4 products. However, without information on
622 their chemical composition and structures, data on P3 and P4 could not be included in Fig. 13.
623 In contrast, the smaller, more volatile P1 products will mainly contribute to particle growth, as
624 suggested by their relatively larger abundance in ESI mass spectra of larger particles (Figs. 7 and
625 S4).

626 Compared to P2 products at m/z 481-543, those with $m/z > 543$ are significantly less
627 important in the flow reactor SOA (geometric mean diameter 13-26 nm), but contribute a greater
628 fraction to total P2 products in the chamber SOA (geometric mean diameter 66 nm). This
629 suggests that these larger P2 products (i.e., $m/z > 543$) play an important role in particle growth
630 and may be formed mainly via condensed phase reactions of P1 products in the SOA.

631 Elemental analysis of SOA from chamber experiments using AMS results in an average O/C
632 ratio of 0.34 ± 0.03 (1σ) and H/C ratio of 1.51 ± 0.02 . These values are within the range given
633 for P1 products detected by ESI-MS (Table 2) and are consistent with our observation that P1
634 products predominantly contribute to particle growth. Along with the potential mechanisms

635 discussed above to explain the formation of observed P1 and P2 products and their contribution
636 to particle formation and growth, another mechanism considered for particle formation and
637 growth is the production of extremely low-volatility organic compounds (ELVOCs), which was
638 proposed to occur via sequential intramolecular hydrogen abstraction/O₂ addition of RO₂ radicals
639 (Vereecken et al., 2007; Crouse et al., 2013; Ehn et al., 2014; Rissanen et al., 2015) and shown
640 to play an important role in particle formation and growth from monoterpene oxidation (Zhao et
641 al., 2013; Ehn et al., 2014; Jokinen et al., 2015). Because of the high oxygen content in ELVOCs,
642 particles formed from these compounds are expected to have high O/C ratios. The ELVOC
643 mechanism cannot be ruled out as being involved in initial particle formation during α -cedrene
644 ozonolysis. However, based on the O/C ratios measured for chamber SOA, it is unlikely to be a
645 dominant contributor to total particle mass in this system. Measurements by AMS are not
646 possible for the flow reactor experiments as the particles are too small to be efficiently
647 transmitted into the AMS.

648 It is clear from the impact of formic acid on particle formation that the SCI plays a key role
649 in forming the HMW products and new particles. In the case of the *trans*-3-hexene ozonolysis
650 (Sadezky et al., 2008; Zhao et al., 2015), the composition of the SOA clearly showed evidence
651 for oligomer formation from the sequential reaction of RO₂ radicals with SCI, leading to ESI
652 mass spectra that showed the repeat unit of oligomers corresponding to SCI. A search for similar
653 products in the α -cedrene reaction was not successful, indicating that while this may contribute,
654 other mechanisms are more important (Zhao et al., 2015). This is not surprising, given the
655 number of potential reaction paths for the SCI from α -cedrene (e.g. Fig. S9) and the large
656 number of low volatility products that can quickly contribute to growth and the SOA
657 composition once nucleation has occurred.

658 The incorporation of 2-EHN into SOA and its very slow evaporation back out (Figs. 4 and 5)
659 is consistent with a condensation type of growth mechanism (Finlayson-Pitts and Pitts, 2000;
660 Seinfeld and Pandis, 2006) in which organic species are irreversibly taken up by the particle
661 surface and thus their incorporation into particles depends on the collision frequency of the gas
662 with the particle surface and the magnitude of the uptake coefficient (Perraud et al., 2012). Such
663 a growth mechanism is characteristic of highly viscous SOA, in which incorporated organic
664 species undergo very slow evaporation because of the diffusion limitation, in contrast to an

665 equilibrium mechanism that applies for low-viscosity liquid particles. This result also suggests
666 that growth will occur not only via low volatility products but also via uptake of higher volatility
667 species such as the smaller P1 products identified here.

668 **4. Summary**

669 The present study examines the phase state and mechanisms of formation and growth of SOA
670 from ozonolysis of α -cedrene. The SOA is characterized to be a high-viscosity semi-solid, with
671 an estimated diffusion coefficient of $3 \times 10^{-15} \text{ cm}^2 \text{ s}^{-1}$ for 2-EHN that was incorporated into the
672 SOA during ozonolysis. High molecular weight products, tentatively identified mainly as aldol
673 condensation products, peroxyhemiacetals, and esters, comprise a significant fraction of SOA.
674 The size-dependent distribution of these products in the SOA as well as their positive correlation
675 with new particle formation suggests that they are responsible for initial particle formation, in
676 contrast to lower molecular weight (P1) products that mainly contribute to particle growth via a
677 kinetic condensation mechanism.

678 Bonn and Moortgat (2003) have suggested that sesquiterpene ozonolysis could be one source
679 of new particle formation in the boreal forest. Evidence for the role of sesquiterpenes in
680 atmospheric new particle formation has been recently presented by field observations in the
681 boreal forest in Finland (Bonn et al., 2008) and in the Front Range of the Colorado Rocky
682 Mountains (Boy et al., 2008). These studies have proposed possible nucleation mechanisms
683 involving low-volatility products such as intermolecularly formed SOZ and organosulfates from
684 sesquiterpene oxidation. The results of the present study suggest that the formation of HMW
685 products during ozonolysis may serve as an important mechanism for such new particle
686 formation.

687 Mechanisms of ozonolysis of alkenes and in particular, the pathways that lead to SOA
688 formation are highly dependent on the size and structure of the parent alkene. However, in all
689 cases stabilized Criegee intermediates play a key role. For example, SOA generated from
690 ozonolysis of small alkenes such as *trans*-3-hexene is primarily composed of oligomers formed
691 from the sequential addition of SCI to RO_2 radicals (Sadezky et al., 2008; Zhao et al., 2015). For
692 larger alkenes, such as α -cedrene, the SCI react via multiple pathways, leading to a variety of
693 low volatility products (e.g., P2 and newly observed P1 products) that can nucleate on their own

694 to form new particles. There is yet a third group of alkenes with intermediate molecular sizes
695 such as monoterpenes, for which the major first generation ozonolysis products do not have low
696 enough volatilities to nucleate on their own (Hallquist et al., 2009) and therefore the ELVOC
697 mechanism, despite the small yields (a few percent, Jokinen et al., 2015), may play a more
698 dominant role (Zhao et al., 2013; Ehn et al., 2014). The dependence of phase, composition, and
699 mechanisms for particle formation and growth should be taken into account in atmospheric
700 models of the formation and impacts of SOA on visibility, human health, and climate.

701 **Acknowledgements**

702 This work was supported by the National Science Foundation (Grants #1207112) and the NSF
703 Major Research Instrumentation (MRI) program (Grant # 0923323 and 1337080). The authors
704 are grateful to John Greaves, Beniam Berhane, and Shirin Sorooshian for their help with accurate
705 mass measurements.

706 **References**

- 707 Abramson, E., Imre, D., Beranek, J., Wilson, J., and Zelenyuk, A.: Experimental determination
708 of chemical diffusion within secondary organic aerosol particles, *Phys. Chem. Chem.*
709 *Phys.*, 15, 2983-2991, doi:10.1039/C2cp44013j, 2013.
- 710 Alfarra, M. R., Hamilton, J. F., Wyche, K. P., Good, N., Ward, M. W., Carr, T., Barley, M. H.,
711 Monks, P. S., Jenkin, M. E., Lewis, A. C., and McFiggans, G. B.: The effect of
712 photochemical ageing and initial precursor concentration on the composition and
713 hygroscopic properties of beta-caryophyllene secondary organic aerosol, *Atmos. Chem.*
714 *Phys.*, 12, 6417-6436, doi:10.5194/acp-12-6417-2012, 2012.
- 715 Anglada, J. M., Gonzalez, J., and Torrent-Sucarrat, M.: Effects of the substituents on the
716 reactivity of carbonyl oxides. A theoretical study on the reaction of substituted carbonyl
717 oxides with water, *Phys. Chem. Chem. Phys.*, 13, 13034-13045, doi:10.1039/c1cp20872a,
718 2011.
- 719 Bateman, A. P., Bertram, A. K., and Martin, S. T.: Hygroscopic Influence on the Semisolid-to-
720 Liquid Transition of Secondary Organic Materials, *J. Phys. Chem. A*, 119, 4386-4395,
721 doi:10.1021/jp508521c, 2015.
- 722 Berndt, T., Kaethner, R., Voigtlander, J., Stratmann, F., Pfeifle, M., Reichle, P., Sipila, M.,
723 Kulmala, M., and Olzmann, M.: Kinetics of the unimolecular reaction of CH₂OO and the
724 bimolecular reactions with the water monomer, acetaldehyde and acetone under
725 atmospheric conditions, *Phys. Chem. Chem. Phys.*, 17, 19862-19873, doi:
726 10.1039/c5cp02224j, 2015.
- 727 Birdsall, A. W., Zentner, C. A., and Elrod, M. J.: Study of the kinetics and equilibria of the
728 oligomerization reactions of 2-methylglyceric acid, *Atmos. Chem. Phys.*, 13, 3097-3109,
729 doi:10.5194/acp-13-3097-2013, 2013.
- 730 Bones, D. L., Reid, J. P., Lienhard, D. M., and Krieger, U. K.: Comparing the mechanism of
731 water condensation and evaporation in glassy aerosol, *Proc. Natl. Acad. Sci. U. S. A.*, 109,
732 11613-11618, 2012.
- 733 Bonn, B., and Moortgat, G. K.: Sesquiterpene ozonolysis: Origin of atmospheric new particle
734 formation from biogenic hydrocarbons, *Geophys. Res. Lett.*, 30, 1585,
735 doi:10.1029/2003GL017000, 2003.
- 736 Bonn, B., Kulmala, M., Riipinen, I., Sihto, S. L., and Ruuskanen, T. M.: How biogenic terpenes
737 govern the correlation between sulfuric acid concentrations and new particle formation, *J.*
738 *Geophys. Res.*, 113, D12209, doi:10.1029/2007jd009327, 2008.
- 739 Bouvier-Brown, N. C., Goldstein, A. H., Gilman, J. B., Kuster, W. C., and de Gouw, J. A.: In-situ
740 ambient quantification of monoterpenes, sesquiterpenes, and related oxygenated
741 compounds during BEARPEX 2007: implications for gas- and particle-phase chemistry,
742 *Atmos. Chem. Phys.*, 9, 5505-5518, 2009.
- 743 Boy, M., Karl, T., Turnipseed, A., Mauldin, R. L., Kosciuch, E., Greenberg, J., Rathbone, J.,
744 Smith, J., Held, A., Barsanti, K., Wehner, B., Bauer, S., Wiedensohler, A., Bonn, B.,
745 Kulmala, M., and Guenther, A.: New particle formation in the front range of the colorado
746 rocky mountains, *Atmos. Chem. Phys.*, 8, 1577-1590, 2008.
- 747 Bruns, E. A., Perraud, V., Zelenyuk, A., Ezell, M. J., Johnson, S. N., Yu, Y., Imre, D., Finlayson-
748 Pitts, B. J., and Alexander, M. L.: Comparison of FTIR and particle mass spectrometry
749 for the measurement of particulate organic nitrates, *Environ. Sci. Technol.*, 44, 1056-1061,
750 doi:10.1021/Es9029864, 2010.

751 Canagaratna, M. R., Jimenez, J. L., Kroll, J. H., Chen, Q., Kessler, S. H., Massoli, P., Ruiz, L. H.,
752 Fortner, E., Williams, L. R., Wilson, K. R., Surratt, J. D., Donahue, N. M., Jayne, J. T.,
753 and Worsnop, D. R.: Elemental ratio measurements of organic compounds using aerosol
754 mass spectrometry: characterization, improved calibration, and implications, *Atmos.*
755 *Chem. Phys.*, 15, 253-272, doi:10.5194/acp-15-253-2015, 2015.

756 Cappa, C. D., and Wilson, K. R.: Evolution of organic aerosol mass spectra upon heating:
757 implications for OA phase and partitioning behavior, *Atmos. Chem. Phys.*, 11, 1895-1911,
758 doi:10.5194/acp-11-1895-2011, 2011.

759 Chan, M. N., Surratt, J. D., Chan, A. W. H., Schilling, K., Offenberg, J. H., Lewandowski, M.,
760 Edney, E. O., Kleindienst, T. E., Jaoui, M., Edgerton, E. S., Tanner, R. L., Shaw, S. L.,
761 Zheng, M., Knipping, E. M., and Seinfeld, J. H.: Influence of aerosol acidity on the
762 chemical composition of secondary organic aerosol from beta-caryophyllene, *Atmos.*
763 *Chem. Phys.*, 11, 1735-1751, doi:10.5194/acp-11-1735-2011, 2011.

764 Chan, M. N., Zhang, H. F., Goldstein, A. H., and Wilson, K. R.: Role of water and phase in the
765 heterogeneous oxidation of solid and aqueous succinic acid aerosol by hydroxyl radicals,
766 *J. Phys. Chem. C*, 118, 28978-28992, doi:10.1021/jp5012022, 2014.

767 Chao, W., Hsieh, J. T., Chang, C. H., and Lin, J. J. M.: Direct kinetic measurement of the
768 reaction of the simplest Criegee intermediate with water vapor, *Science*, 347, 751-754,
769 doi:10.1126/science.1261549, 2015.

770 Chen, Q., Li, Y. L., McKinney, K. A., Kuwata, M., and Martin, S. T.: Particle mass yield from
771 beta-caryophyllene ozonolysis, *Atmos. Chem. Phys.*, 12, 3165-3179, doi:10.5194/acp-12-
772 3165-2012, 2012.

773 Cody, R. B., Laramee, J. A., and Durst, H. D.: Versatile new ion source for the analysis of
774 materials in open air under ambient conditions, *Anal. Chem.*, 77, 2297-2302,
775 doi:10.1021/ac050162j, 2005.

776 Compernelle, S., Ceulemans, K., and Muller, J. F.: EVAPORATION: A new vapour pressure
777 estimation method for organic molecules including non-additivity and intramolecular
778 interactions, *Atmos. Chem. Phys.*, 11, 9431-9450, 2011.

779 Crank, J.: *The mathematics of diffusion*, 2nd ed., Clarendon Press, Oxford, [Eng], 1975.

780 Crouse, J. D., Nielsen, L. B., Jorgensen, S., Kjaergaard, H. G., and Wennberg, P. O.:
781 Autoxidation of organic compounds in the atmosphere, *J. Phys. Chem. Lett.*, 4, 3513-
782 3520, 2013.

783 DeCarlo, P. F., Kimmel, J. R., Trimborn, A., Northway, M. J., Jayne, J. T., Aiken, A. C., Gonin,
784 M., Fuhrer, K., Horvath, T., Docherty, K. S., Worsnop, D. R., and Jimenez, J. L.: Field-
785 deployable, high-resolution, time-of-flight aerosol mass spectrometer, *Anal. Chem.*, 78,
786 8281-8289, 2006.

787 DePalma, J. W., Horan, A. J., Hall, W. A., and Johnston, M. V.: Thermodynamics of oligomer
788 formation: implications for secondary organic aerosol formation and reactivity, *Phys.*
789 *Chem. Chem. Phys.*, 15, 6935-6944, 2013.

790 Ding, X., He, Q. F., Shen, R. Q., Yu, Q. Q., and Wang, X. M.: Spatial distributions of secondary
791 organic aerosols from isoprene, monoterpenes, beta-caryophyllene, and aromatics over
792 China during summer, *J. Geophys. Res.*, 119, 11877-11891, Doi 10.1002/2014jd021748,
793 2014.

794 Docherty, K. S., Wu, W., Lim, Y. B., and Ziemann, P. J.: Contributions of organic peroxides to
795 secondary aerosol formed from reactions of monoterpenes with O₃, *Environ. Sci.*
796 *Technol.*, 39, 4049-4059, 2005.

797 Donahue, N. M., Drozd, G. T., Epstein, S. A., Presto, A. A., and Kroll, J. H.: Adventures in
798 ozoneland: down the rabbit-hole, *Phys. Chem. Chem. Phys.*, 13, 10848-10857,
799 doi:10.1039/c0cp02564j, 2011.

800 Donahue, N. M., Ortega, I. K., Chuang, W., Riipinen, I., Riccobono, F., Schobesberger, S.,
801 Dommen, J., Baltensperger, U., Kulmala, M., Worsnop, D. R., and Vehkamäki, H.: How
802 do organic vapors contribute to new-particle formation?, *Faraday Discuss.*, 165, 91-104,
803 doi:10.1039/c3fd00046j, 2013.

804 Duhl, T. R., Helmig, D., and Guenther, A.: Sesquiterpene emissions from vegetation: a review,
805 *Biogeosciences*, 5, 761-777, 2008.

806 Ehn, M., Thornton, J. A., Kleist, E., Sipila, M., Junninen, H., Pullinen, I., Springer, M., Rubach,
807 F., Tillmann, R., Lee, B., Lopez-Hilfiker, F., Andres, S., Acir, I. H., Rissanen, M., Jokinen,
808 T., Schobesberger, S., Kangasluoma, J., Kontkanen, J., Nieminen, T., Kurten, T., Nielsen,
809 L. B., Jorgensen, S., Kjaergaard, H. G., Canagaratna, M., Dal Maso, M., Berndt, T., Petaja,
810 T., Wahner, A., Kerminen, V. M., Kulmala, M., Worsnop, D. R., Wildt, J., and Mentel, T.
811 F.: A large source of low-volatility secondary organic aerosol, *Nature*, 506, 476-479, 2014.

812 Finlayson-Pitts, B. J., and Pitts, J. N.: *Chemistry of the upper and lower atmosphere: theory,*
813 *experiments, and applications*, Academic Press, San Diego, 2000.

814 Gao, Y. Q., Hall, W. A., and Johnston, M. V.: Molecular composition of monoterpene secondary
815 organic aerosol at low mass loading, *Environ. Sci. Technol.*, 44, 7897-7902,
816 doi:10.1021/Es101861k, 2010.

817 Goldstein, A. H., and Galbally, I. E.: Known and unexplored organic constituents in the earth's
818 atmosphere, *Environ. Sci. Technol.*, 41, 1514-1521, doi:10.1021/Es072476p, 2007.

819 Greaves, J., and Roboz, J.: *Mass spectrometry for the novice*, CRC Press, Boca Raton, F. L.,
820 USA, 2013.

821 Guenther, A., Hewitt, C. N., Erickson, D., Fall, R., Geron, C., Graedel, T., Harley, P., Klinger, L.,
822 Lerdau, M., McKay, W. A., Pierce, T., Scholes, B., Steinbrecher, R., Tallamraju, R., Taylor,
823 J., and Zimmerman, P.: A global-model of natural volatile organic compound emissions, *J.*
824 *Geophys. Res.*, 100, 8873-8892, doi:10.1029/94jd02950, 1995.

825 Hall, W. A., and Johnston, M. V.: Oligomer formation pathways in secondary organic aerosol
826 from MS and MS/MS measurements with high mass accuracy and resolving power, *J.*
827 *Am. Soc. Mass Spectrom.*, 23, 1097-1108, 2012.

828 Hallquist, M., Wenger, J. C., Baltensperger, U., Rudich, Y., Simpson, D., Claeys, M., Dommen, J.,
829 Donahue, N. M., George, C., Goldstein, A. H., Hamilton, J. F., Herrmann, H., Hoffmann,
830 T., Iinuma, Y., Jang, M., Jenkin, M. E., Jimenez, J. L., Kiendler-Scharr, A., Maenhaut, W.,
831 McFiggans, G., Mentel, T. F., Monod, A., Prevot, A. S. H., Seinfeld, J. H., Surratt, J. D.,
832 Szmigielski, R., and Wildt, J.: The formation, properties and impact of secondary organic
833 aerosol: current and emerging issues, *Atmos. Chem. Phys.*, 9, 5155-5236, 2009.

834 Harrick, N. J.: *Internal reflection spectroscopy*, Interscience Publishers, New York, 1967.

835 Heaton, K. J., Slighter, R. L., Hatcher, P. G., Hall, W. A., and Johnston, M. V.: Composition
836 domains in monoterpene secondary organic aerosol, *Environ. Sci. Technol.*, 43, 7797-
837 7802, 2009.

838 Helmig, D., Ortega, J., Duhl, T., Tanner, D., Guenther, A., Harley, P., Wiedinmyer, C., Milford, J.,
839 and Sakulyanontvittaya, T.: Sesquiterpene emissions from pine trees - Identifications,
840 emission rates and flux estimates for the contiguous United States, *Environ. Sci. Technol.*,
841 41, 1545-1553, doi:10.1021/Es0618907, 2007.

842 Hodas, N., Zuend, A., Mui, W., Flagan, R. C., and Seinfeld, J. H.: Influence of particle-phase

843 state on the hygroscopic behavior of mixed organic-inorganic aerosols, *Atmos. Chem.*
844 *Phys.*, 15, 5027-5045, doi:10.5194/acp-15-5027-2015, 2015.

845 Hoffmann, T., Odum, J. R., Bowman, F., Collins, D., Klockow, D., Flagan, R. C., and Seinfeld, J.
846 H.: Formation of organic aerosols from the oxidation of biogenic hydrocarbons, *J. Atmos.*
847 *Chem.*, 26, 189-222, doi:10.1023/A:1005734301837, 1997.

848 Hoffmann, T., Bandur, R., Marggraf, U., and Linscheid, M.: Molecular composition of organic
849 aerosols formed in the alpha-pinene/O₃ reaction: Implications for new particle formation
850 processes, *J. Geophys. Res.*, 103, 25569-25578, 1998.

851 Hu, D., Bian, Q., Li, T. W. Y., Lau, A. K. H., and Yu, J. Z.: Contributions of isoprene,
852 monoterpenes, beta-caryophyllene, and toluene to secondary organic aerosols in Hong
853 Kong during the summer of 2006, *J. Geophys. Res.*, 113, D22206,
854 doi:10.1029/2008jd010437, 2008.

855 IPCC: Summary for Policymakers. In: *Climate Change 2013: The Physical Science Basis.*
856 *Contribution of Working Group I to the Fifth Assessment Report of the*
857 *Intergovernmental Panel on Climate Change [Stocker, T.F., D. Qin, G.-K. Plattner, M.*
858 *Tignor, S.K. Allen, J. Boschung, A. Nauels, Y. Xia, V. Bex and P.M. Midgley (eds.)].*
859 *Cambridge University Press, Cambridge, United Kingdom and New York, NY, USA.,*
860 *2013.*

861 Jaoui, M., Sexton, K. G., and Kamens, R. M.: Reaction of alpha-cedrene with ozone: mechanism,
862 gas and particulate products distribution, *Atmos. Environ.*, 38, 2709-2725, 2004.

863 Jaoui, M., Kleindienst, T. E., Docherty, K. S., Lewandowski, M., and Offenberg, J. H.:
864 Secondary organic aerosol formation from the oxidation of a series of sesquiterpenes:
865 alpha-cedrene, beta-caryophyllene, alpha-humulene and alpha-farnesene with O₃, OH and
866 NO₃ radicals, *Environ. Chem.*, 10, 178-193, doi:10.1071/En13025, 2013.

867 Jokinen, T., Berndt, T., Makkonen, R., Kerminen, V. M., Junninen, H., Paasonen, P., Stratmann,
868 F., Herrmann, H., Guenther, A. B., Worsnop, D. R., Kulmala, M., Ehn, M., and Sipila, M.:
869 Production of extremely low volatile organic compounds from biogenic emissions:
870 Measured yields and atmospheric implications, *Proc. Natl. Acad. Sci. U. S. A.*, 112, 7123-
871 7128, doi:10.1073/pnas.1423977112, 2015.

872 Kanakidou, M., Seinfeld, J. H., Pandis, S. N., Barnes, I., Dentener, F. J., Facchini, M. C., Van
873 Dingenen, R., Ervens, B., Nenes, A., Nielsen, C. J., Swietlicki, E., Putaud, J. P.,
874 Balkanski, Y., Fuzzi, S., Horth, J., Moortgat, G. K., Winterhalter, R., Myhre, C. E. L.,
875 Tsigaridis, K., Vignati, E., Stephanou, E. G., and Wilson, J.: Organic aerosol and global
876 climate modelling: a review, *Atmos. Chem. Phys.*, 5, 1053-1123, 2005.

877 Kanawati, B., Herrmann, F., Joniec, S., Winterhalter, R., and Moortgat, G. K.: Mass
878 spectrometric characterization of beta-caryophyllene ozonolysis products in the aerosol
879 studied using an electrospray triple quadrupole and time-of-flight analyzer hybrid system
880 and density functional theory, *Rapid Commun. Mass Spectrom.*, 22, 165-186,
881 doi:10.1002/Rcm.3340, 2008.

882 Kidd, C., Perraud, V., and Finlayson-Pitts, B. J.: New insights into secondary organic aerosol
883 from the ozonolysis of alpha-pinene from combined infrared spectroscopy and mass
884 spectrometry measurements, *Phys. Chem. Chem. Phys.*, 16, 22706-22716, 2014a.

885 Kidd, C., Perraud, V., Wingen, L. M., and Finlayson-Pitts, B. J.: Integrating phase and
886 composition of secondary organic aerosol from the ozonolysis of alpha-pinene, *Proc. Natl.*
887 *Acad. Sci. U. S. A.*, 111, 7552-7557, 2014b.

888 Kim, H., Liu, S., Russell, L. M., and Paulson, S. E.: Dependence of real refractive indices on

889 O:C, H:C and mass fragments of secondary organic aerosol generated from ozonolysis
890 and photooxidation of limonene and alpha-pinene, *Aerosol Sci. Technol.*, 48, 498-507,
891 doi:10.1080/02786826.2014.893278, 2014.

892 Koop, T., Bookhold, J., Shiraiwa, M., and Poschl, U.: Glass transition and phase state of organic
893 compounds: dependency on molecular properties and implications for secondary organic
894 aerosols in the atmosphere, *Phys. Chem. Chem. Phys.*, 13, 19238-19255, 2011.

895 Kristensen, K., Enggrob, K. L., King, S. M., Worton, D. R., Platt, S. M., Mortensen, R.,
896 Rosenoern, T., Surratt, J. D., Bilde, M., Goldstein, A. H., and Glasius, M.: Formation and
897 occurrence of dimer esters of pinene oxidation products in atmospheric aerosols, *Atmos.*
898 *Chem. Phys.*, 13, 3763-3776, 2013.

899 Kristensen, K., Cui, T., Zhang, H., Gold, A., Glasius, M., and Surratt, J. D.: Dimers in alpha-
900 pinene secondary organic aerosol: effect of hydroxyl radical, ozone, relative humidity and
901 aerosol acidity, *Atmos. Chem. Phys.*, 14, 4201-4218, 2014.

902 Kroll, J. H., and Seinfeld, J. H.: Chemistry of secondary organic aerosol: Formation and
903 evolution of low-volatility organics in the atmosphere, *Atmos. Environ.*, 42, 3593-3624,
904 2008.

905 Lambe, A. T., Cappa, C. D., Massoli, P., Onasch, T. B., Forestieri, S. D., Martin, A. T.,
906 Cummings, M. J., Croasdale, D. R., Brune, W. H., Worsnop, D. R., and Davidovits, P.:
907 Relationship between oxidation level and optical properties of secondary organic aerosol,
908 *Environ. Sci. Technol.*, 47, 6349-6357, 2013.

909 Lee, A., Goldstein, A. H., Keywood, M. D., Gao, S., Varutbangkul, V., Bahreini, R., Ng, N. L.,
910 Flagan, R. C., and Seinfeld, J. H.: Gas-phase products and secondary aerosol yields from
911 the ozonolysis of ten different terpenes, *J. Geophys. Res.*, 111, D07302,
912 10.1029/2005JD006437, 2006.

913 Lee, C. T., and Kamens, R. M.: Particle nucleation from the reaction of α -pinene and O₃, *Atmos.*
914 *Env.*, 39, 6822-6832, 2005.

915 Lewis, T. R., Blitz, M. A., Heard, D. E., and Seakins, P. W.: Direct evidence for a substantive
916 reaction between the Criegee intermediate, CH₂OO, and the water vapour dimer, *Phys.*
917 *Chem. Chem. Phys.*, 17, 4859-4863, doi:10.1039/c4cp04750h, 2015.

918 Li, Y. J., Chen, Q., Guzman, M. I., Chan, C. K., and Martin, S. T.: Second-generation products
919 contribute substantially to the particle-phase organic material produced by beta-
920 caryophyllene ozonolysis, *Atmos. Chem. Phys.*, 11, 121-132, doi:10.5194/acp-11-121-
921 2011, 2011.

922 Lignell, H., Hinks, M. L., and Nizkorodov, S. A.: Exploring matrix effects on photochemistry of
923 organic aerosols, *Proc. Natl. Acad. Sci. U. S. A.*, 111, 13780-13785, 2014.

924 Mauderly, J. L., and Chow, J. C.: Health effects of organic aerosols, *Inhalation Toxicol.*, 20, 257-
925 288, doi:10.1080/08958370701866008, 2008.

926 Mehrer, H.: Diffusion in solids: fundamentals, methods, materials, diffusion-controlled processes,
927 Springer series in solid state science, 155, Springer, Berlin; New York, 2007.

928 Mikhailov, E., Vlasenko, S., Martin, S. T., Koop, T., and Poschl, U.: Amorphous and crystalline
929 aerosol particles interacting with water vapor: conceptual framework and experimental
930 evidence for restructuring, phase transitions and kinetic limitations, *Atmos. Chem. Phys.*,
931 9, 9491-9522, 2009.

932 Muller, L., Reinnig, M. C., Warnke, J., and Hoffmann, T.: Unambiguous identification of esters
933 as oligomers in secondary organic aerosol formed from cyclohexene and
934 cyclohexene/alpha-pinene ozonolysis, *Atmos. Chem. Phys.*, 8, 1423-1433, 2008.

935 Muller, L., Reinnig, M. C., Hayen, H., and Hoffmann, T.: Characterization of oligomeric
936 compounds in secondary organic aerosol using liquid chromatography coupled to
937 electrospray ionization Fourier transform ion cyclotron resonance mass spectrometry,
938 *Rapid Commun. Mass Spectrom.*, 23, 971-979, 2009.

939 Nah, T., Chan, M., Leone, S. R., and Wilson, K. R.: Real time in situ chemical characterization
940 of submicrometer organic particles using direct analysis in real time-mass spectrometry,
941 *Anal. Chem.*, 85, 2087-2095, doi:10.1021/ac302560c, 2013.

942 Ng, N. L., Kroll, J. H., Keywood, M. D., Bahreini, R., Varutbangkul, V., Flagan, R. C., Seinfeld,
943 J. H., Lee, A., and Goldstein, A. H.: Contribution of first- versus second-generation
944 products to secondary organic aerosols formed in the oxidation of biogenic hydrocarbons,
945 *Environ. Sci. Technol.*, 40, 2283-2297, doi:10.1021/Es052269u, 2006.

946 Pajunoja, A., Lambe, A. T., Hakala, J., Rastak, N., Cummings, M. J., Brogan, J. F., Hao, L. Q.,
947 Paramonov, M., Hong, J., Prisle, N. L., Malila, J., Romakkaniemi, S., Lehtinen, K. E. J.,
948 Laaksonen, A., Kulmala, M., Massoli, P., Onasch, T. B., Donahue, N. M., Riipinen, I.,
949 Davidovits, P., Worsnop, D. R., Petaja, T., and Virtanen, A.: Adsorptive uptake of water
950 by semisolid secondary organic aerosols, *Geophys. Res. Lett.*, 42, 3063-3068,
951 doi:10.1002/2015GL063142, 2015.

952 Pankow, J. F., and Asher, W. E.: SIMPOL.1: a simple group contribution method for predicting
953 vapor pressures and enthalpies of vaporization of multifunctional organic compounds,
954 *Atmos. Chem. Phys.*, 8, 2773-2796, 2008.

955 Perraud, V., Bruns, E. A., Ezell, M. J., Johnson, S. N., Yu, Y., Alexander, M. L., Zelenyuk, A.,
956 Imre, D., Chang, W. L., Dabdub, D., Pankow, J. F., and Finlayson-Pitts, B. J.:
957 Nonequilibrium atmospheric secondary organic aerosol formation and growth, *Proc. Natl.*
958 *Acad. Sci. U. S. A.*, 109, 2836-2841, 2012.

959 Reinnig, M. C., Warnke, J., and Hoffmann, T.: Identification of organic hydroperoxides and
960 hydroperoxy acids in secondary organic aerosol formed during the ozonolysis of different
961 monoterpenes and sesquiterpenes by on-line analysis using atmospheric pressure
962 chemical ionization ion trap mass spectrometry, *Rapid Commun. Mass Spectrom.*, 23,
963 1735-1741, doi:10.1002/Rcm.4065, 2009.

964 Renbaum-Wolff, L., Grayson, J. W., Bateman, A. P., Kuwata, M., Sellier, M., Murray, B. J.,
965 Shilling, J. E., Martin, S. T., and Bertram, A. K.: Viscosity of alpha-pinene secondary
966 organic material and implications for particle growth and reactivity, *Proc. Natl. Acad. Sci.*
967 *U. S. A.*, 110, 8014-8019, 2013.

968 Renbaum, L. H., and Smith, G. D.: The importance of phase in the radical-initiated oxidation of
969 model organic aerosols: reactions of solid and liquid brassidic acid particles, *Phys. Chem.*
970 *Chem. Phys.*, 11, 2441-2451, doi:10.1039/b816799k, 2009.

971 Richters, S., Herrmann, H., and Berndt, T.: Gas-phase rate coefficients of the reaction of ozone
972 with four sesquiterpenes at 295 +/- 2 K, *Phys. Chem. Chem. Phys.*, 17, 11658-11669,
973 doi:10.1039/c4cp05542j, 2015.

974 Riipinen, I., Pierce, J. R., Yli-Juuti, T., Nieminen, T., Hakkinen, S., Ehn, M., Junninen, H.,
975 Lehtipalo, K., Petaja, T., Slowik, J., Chang, R., Shantz, N. C., Abbatt, J., Leaitch, W. R.,
976 Kerminen, V. M., Worsnop, D. R., Pandis, S. N., Donahue, N. M., and Kulmala, M.:
977 Organic condensation: a vital link connecting aerosol formation to cloud condensation
978 nuclei (CCN) concentrations, *Atmos. Chem. Phys.*, 11, 3865-3878, doi:10.5194/acp-11-
979 3865-2011, 2011.

980 Rissanen, M. P., Kurten, T., Sipila, M., Thornton, J. A., Kausiala, O., Garmash, O., Kjaergaard, H.

981 G., Petaja, T., Worsnop, D. R., Ehn, M., and Kulmala, M.: Effects of chemical complexity
982 on the autoxidation mechanisms of endocyclic alkene ozonolysis products: from
983 methylcyclohexenes toward understanding alpha-pinene, *J. Phys. Chem. A*, 119, 4633-
984 4650, doi:10.1021/jp510966g, 2015.

985 Ruscic, B.: Active thermochemical tables: water and water dimer, *J. Phys. Chem. A*, 117, 11940-
986 11953, doi:10.1021/jp403197t, 2013.

987 Ryzhkov, A. B., and Ariya, P. A.: A theoretical study of the reactions of parent and substituted
988 Criegee intermediates with water and the water dimer, *Phys. Chem. Chem. Phys.*, 6,
989 5042-5050, doi:10.1039/b408414d, 2004.

990 Sadezky, A., Winterhalter, R., Kanawati, B., Rompp, A., Spengler, B., Mellouki, A., Le Bras, G.,
991 Chaimbault, P., and Moortgat, G. K.: Oligomer formation during gas-phase ozonolysis of
992 small alkenes and enol ethers: new evidence for the central role of the Criegee
993 Intermediate as oligomer chain unit, *Atmos. Chem. Phys.*, 8, 2667-2699, 2008.

994 Sakulyanontvittaya, T., Duhl, T., Wiedinmyer, C., Helmig, D., Matsunaga, S., Potosnak, M.,
995 Milford, J., and Guenther, A.: Monoterpene and sesquiterpene emission estimates for the
996 United States, *Environ. Sci. Technol.*, 42, 1623-1629, doi:10.1021/Es702274e, 2008a.

997 Sakulyanontvittaya, T., Guenther, A., Helmig, D., Milford, J., and Wiedinmyer, C.: Secondary
998 organic aerosol from sesquiterpene and monoterpene emissions in the United States,
999 *Environ. Sci. Technol.*, 42, 8784-8790, doi:10.1021/Es800817r, 2008b.

1000 Saukko, E., Lambe, A. T., Massoli, P., Koop, T., Wright, J. P., Croasdale, D. R., Pedernera, D. A.,
1001 Onasch, T. B., Laaksonen, A., Davidovits, P., Worsnop, D. R., and Virtanen, A.:
1002 Humidity-dependent phase state of SOA particles from biogenic and anthropogenic
1003 precursors, *Atmos. Chem. Phys.*, 12, 7517-7529, doi:10.5194/acp-12-7517-2012, 2012.

1004 Seinfeld, J. H., and Pandis, S. N.: Atmospheric chemistry and physics: from air pollution to
1005 climate change, 2nd ed., J. Wiley, Hoboken, N.J., 2006.

1006 Shiraiwa, M., Ammann, M., Koop, T., and Poschl, U.: Gas uptake and chemical aging of
1007 semisolid organic aerosol particles, *Proc. Natl. Acad. Sci. U. S. A.*, 108, 11003-11008,
1008 2011.

1009 Shiraiwa, M., and Seinfeld, J. H.: Equilibration timescale of atmospheric secondary organic
1010 aerosol partitioning, *Geophys. Res. Lett.*, 39, L24801, doi:10.1029/2012GL054008, 2012.

1011 Shiraiwa, M., Selzle, K., and Poschl, U.: Hazardous components and health effects of
1012 atmospheric aerosol particles: reactive oxygen species, soot, polycyclic aromatic
1013 compounds and allergenic proteins, *Free Radical Res.*, 46, 927-939,
1014 doi:10.3109/10715762.2012.663084, 2012.

1015 Shu, Y. G., and Atkinson, R.: Rate constants for the gas-phase reactions of O₃ with a series of
1016 terpenes and OH radical formation from the O₃ reactions with sesquiterpenes at 296±2
1017 K, *Int. J. Chem. Kinet.*, 26, 1193-1205, 1994.

1018 Slade, J. H., and Knopf, D. A.: Multiphase OH oxidation kinetics of organic aerosol: The role of
1019 particle phase state and relative humidity, *Geophys. Res. Lett.*, 41, 5297-5306,
1020 doi:10.1002/2014GL060582, 2014.

1021 Socrates, G.: Infrared and Raman characteristic group frequencies: tables and charts, 3rd ed.,
1022 Wiley, Chichester; New York, 2001.

1023 Taatjes, C. A., Welz, O., Eskola, A. J., Savee, J. D., Scheer, A. M., Shallcross, D. E., Rotavera, B.,
1024 Lee, E. P. F., Dyke, J. M., Mok, D. K. W., Osborn, D. L., and Percival, C. J.: Direct
1025 measurements of conformer-dependent reactivity of the criegee intermediate CH₃CHOO,
1026 *Science*, 340, 177-180, 2013.

1027 Tasoglou, A., and Pandis, S. N.: Formation and chemical aging of secondary organic aerosol
1028 during the beta-caryophyllene oxidation, *Atmos. Chem. Phys.*, 15, 6035-6046,
1029 doi:10.5194/acp-15-6035-2015, 2015.

1030 Tolocka, M. P., Jang, M., Ginter, J. M., Cox, F. J., Kamens, R. M., and Johnston, M. V.:
1031 Formation of oligomers in secondary organic aerosol, *Environ. Sci. Technol.*, 38, 1428-
1032 1434, 2004.

1033 Vaden, T. D., Imre, D., Beranek, J., Shrivastava, M., and Zelenyuk, A.: Evaporation kinetics and
1034 phase of laboratory and ambient secondary organic aerosol, *Proc. Natl. Acad. Sci. U. S.*
1035 *A.*, 108, 2190-2195, 2011.

1036 Vereecken, L., Muller, J. F., and Peeters, J.: Low-volatility poly-oxygenates in the OH-initiated
1037 atmospheric oxidation of alpha-pinene: impact of non-traditional peroxy radical
1038 chemistry, *Phys. Chem. Chem. Phys.*, 9, 5241-5248, 2007.

1039 Vereecken, L., Harder, H., and Novelli, A.: The reaction of Criegee intermediates with NO, RO₂,
1040 and SO₂, and their fate in the atmosphere, *Phys. Chem. Chem. Phys.*, 14, 14682-14695,
1041 2012.

1042 Virtanen, A., Joutsensaari, J., Koop, T., Kannosto, J., Yli-Pirila, P., Leskinen, J., Makela, J. M.,
1043 Holopainen, J. K., Poschl, U., Kulmala, M., Worsnop, D. R., and Laaksonen, A.: An
1044 amorphous solid state of biogenic secondary organic aerosol particles, *Nature*, 467, 824-
1045 827, doi:10.1038/nature09455, 2010.

1046 Welz, O., Eskola, A. J., Sheps, L., Rotavera, B., Savee, J. D., Scheer, A. M., Osborn, D. L., Lowe,
1047 D., Booth, A. M., Xiao, P., Khan, M. A. H., Percival, C. J., Shallcross, D. E., and Taatjes,
1048 C. A.: Rate coefficients of C1 and C2 Criegee intermediate reactions with formic and
1049 acetic acid near the collision limit: direct kinetics measurements and atmospheric
1050 implications, *Angew. Chem.-Int. Ed.*, 53, 4547-4550, 2014.

1051 Winkler, P. M., Ortega, J., Karl, T., Cappellin, L., Friedli, H. R., Barsanti, K., McMurry, P. H.,
1052 and Smith, J. N.: Identification of the biogenic compounds responsible for size-dependent
1053 nanoparticle growth, *Geophys. Res. Lett.*, 39, L20815, doi:10.1029/2012gl053253, 2012.

1054 Winterhalter, R., Herrmann, F., Kanawati, B., Nguyen, T. L., Peeters, J., Vereecken, L., and
1055 Moortgat, G. K.: The gas-phase ozonolysis of beta-caryophyllene (C₁₅H₂₄). Part I: an
1056 experimental study, *Phys. Chem. Chem. Phys.*, 11, 4152-4172, doi:10.1039/B817824k,
1057 2009.

1058 Witkowski, B., and Gierczak, T.: Analysis of alpha-acyloxyhydroperoxy aldehydes with
1059 electrospray ionization-tandem mass spectrometry (ESI-MSⁿ), *J. Mass Spectrom.*, 48, 79-
1060 88, doi:10.1002/jms.3130, 2013.

1061 Witkowski, B., and Gierczak, T.: Early stage composition of SOA produced by alpha-
1062 pinene/ozone reaction: alpha-Acyloxyhydroperoxy aldehydes and acidic dimers, *Atmos.*
1063 *Environ.*, 95, 59-70, 2014.

1064 Yao, L., Ma, Y., Wang, L., Zheng, J., Khalizov, A., Chen, M. D., Zhou, Y. Y., Qi, L., and Cui, F.
1065 P.: Role of stabilized Criegee intermediate in secondary organic aerosol formation from
1066 the ozonolysis of alpha-cedrene, *Atmos. Environ.*, 94, 448-457, 2014.

1067 Yasmeen, F., Vermeylen, R., Szmigielski, R., Iinuma, Y., Boge, O., Herrmann, H., Maenhaut, W.,
1068 and Claeys, M.: Terpenylic acid and related compounds: precursors for dimers in
1069 secondary organic aerosol from the ozonolysis of alpha- and beta-pinene, *Atmos. Chem.*
1070 *Phys.*, 10, 9383-9392, 2010.

1071 Ying, Q., Li, J. Y., and Kota S. H.: Significant contributions of isoprene to summertime
1072 secondary organic aerosol in eastern United States, *Environ. Sci. Technol.*, 49,

1073 7834–7842, 2015.

1074 Zhang, Q., Jimenez, J. L., Canagaratna, M. R., Allan, J. D., Coe, H., Ulbrich, I., Alfarra, M. R.,
1075 Takami, A., Middlebrook, A. M., Sun, Y. L., Dzepina, K., Dunlea, E., Docherty, K.,
1076 DeCarlo, P. F., Salcedo, D., Onasch, T., Jayne, J. T., Miyoshi, T., Shimojo, A.,
1077 Hatakeyama, S., Takegawa, N., Kondo, Y., Schneider, J., Drewnick, F., Borrmann, S.,
1078 Weimer, S., Demerjian, K., Williams, P., Bower, K., Bahreini, R., Cottrell, L., Griffin, R.
1079 J., Rautiainen, J., Sun, J. Y., Zhang, Y. M., and Worsnop, D. R.: Ubiquity and dominance
1080 of oxygenated species in organic aerosols in anthropogenically-influenced Northern
1081 Hemisphere midlatitudes, *Geophys. Res. Lett.*, 34, L13801, doi:10.1029/2007gl029979,
1082 2007.

1083 Zhang, R. Y., Wang, G. H., Guo, S., Zarnora, M. L., Ying, Q., Lin, Y., Wang, W. G., Hu, M., and
1084 Wang, Y.: Formation of urban fine particulate matter, *Chem. Rev.*, 115, 3803-3855,
1085 doi:10.1021/acs.chemrev.5b00067, 2015.

1086 Zhang, X., McVay, R. C., Huang, D. D., Dalleska, N. F., Aumont, B., Flagan, R. C., and Seinfeld,
1087 J. H.: Formation and evolution of molecular products in α -pinene secondary organic
1088 aerosol, *Proc. Natl. Acad. Sci. U. S. A.*, 112, 14168-14173, doi:
1089 10.1073/pnas.1517742112, 2015.

1090 Zhao, J., Ortega, J., Chen, M., McMurry, P. H., and Smith, J. N.: Dependence of particle
1091 nucleation and growth on high-molecular-weight gas-phase products during ozonolysis of
1092 α -pinene, *Atmos. Chem. Phys.*, 13, 7631-7644, doi:10.5194/acp-13-7631-2013, 2013.

1093 Zhao, Y., Wingen, L. M., Perraud, V., Greaves, J., and Finlayson-Pitts, B. J.: Role of the reaction
1094 of stabilized Criegee intermediates with peroxy radicals in particle formation and growth
1095 in air, *Phys. Chem. Chem. Phys.*, 17, 12500-12514, doi:10.1039/C5cp01171j, 2015.

1096 Ziemann, P. J., and Atkinson, R.: Kinetics, products, and mechanisms of secondary organic
1097 aerosol formation, *Chem. Soc. Rev.*, 41, 6582-6605, 2012.

1098

1099

1100

1101 Table 1 Summary of different types of flow reactor and chamber experiments

| Exp type ^a | [VOC] (ppb) ^b | [O ₃] (ppm) ^c | [HCOOH] or [2-EHN] | RH (%) | Reaction time | Particle size (nm) ^{d, e} | Particle mass conc. (μg m ⁻³) ^e | Particle number conc. (10 ⁶ cm ⁻³) ^e |
|-----------------------|--------------------------|--------------------------------------|--------------------|--------|---------------|------------------------------------|--|--|
| ² FR1 | 138 | 14 | none | < 1 | 27 s | 15.2 ± 0.2 | 26 ± 2 | 7.9 ± 0.2 |
| ² FR2 | 138 | 14 | none | < 1 | 44 s | 22.5 ± 0.8 | 71 ± 8 | 7.0 ± 0.2 |
| ² FR3 | 63 | 16 | none | < 1 | 30 s | 13.1 ± 0.4 | 10 ± 1 | 5.3 ± 0.3 |
| ⁵ FR4 | 138 | 16 | none | < 1 | 30 s | 17.6 ± 0.9 | 52 ± 3 | 9.4 ± 0.3 |
| ² FR5 | 275 | 16 | none | < 1 | 30 s | 25.7 ± 1.1 | 180 ± 16 | 11.8 ± 0.6 |
| ² FR6 | 138 | 16 | none | 75 | 30 s | 16.1 ± 0.9 | 36 ± 10 | 9.3 ± 1.7 |
| ² FR7 | 138 | 16 | 2 ppm HCOOH | < 1 | 30 s | 22.1 ± 0.4 | 41 ± 2 | 2.7 ± 0.1 |
| ² FR8 | 138 | 16 | 15 ppm HCOOH | < 1 | 30 s | 22.0 ± 0.8 | 25 ± 1 | 1.5 ± 0.1 |
| ⁴ CH1 | 34 | 1.5 | none | < 5 | 30 min | 66 ± 2 | 73 ± 6 | 0.34 ± 0.02 |
| ⁴ CH2 | 34 | 1.5 | none | 72 | 30 min | 64 ± 2 | 66 ± 4 | 0.34 ± 0.03 |
| ³ CH3 | 1000 | 0.12 | none | < 5 | 30 min | 111 ± 1 | 363 ± 37 | 0.37 ± 0.03 |
| ³ CH4 | 215 | 1.5 | none | < 5 | 60 min | 140 ± 3 | 984 ± 186 | 0.40 ± 0.02 |
| ² CH5 | 215 | 1.5 | 400 ppb 2-EHN | < 1 | 60 min | 127 ± 5 | 663 ± 44 | 0.35 ± 0.02 |

1102 ^a FR and CH represent flow reactor and chamber experiments, respectively. The numbers in
1103 front of the labels represent the times an experiment was repeated.

1104 ^b The concentrations were calculated from the amount of α -cedrene liquid injected into the flow
1105 reactor and chamber, and the total gas flow.

1106 ^c High O₃ concentration is needed to get enough reaction to form particles in less than a min in
1107 FR experiments.

1108 ^d Geometric mean diameter; the size distributions of SOA formed in the flow reactor are given in
1109 Figs. S1 and 11.

1110 ^e All the data are given as “average value ± one standard deviation”. SOA mass concentrations
1111 are obtained using a particle density of 1.1 g cm⁻³ (Yao et al., 2014). The chamber SOA data are
1112 given for 30 or 60 min reaction times, and were not corrected for the wall loss.

1113 Table 2 Accurate mass and elemental formulae for P1 and P2 products formed from α -cedrene ozonolysis measured by ESI-ToF-MS.

| Product ^a | ESI+ mode ([M+Na] ⁺) | | | | | ESI- mode ([M-H] ⁻) | | | | |
|----------------------|----------------------------------|---|----------------------------|---------------------------|---------------------------|---------------------------------|--|----------------------------|---------------------------|---------------------------|
| | Observed accurate mass (Da) | Elemental formula | Calculated exact mass (Da) | Absolute mass error (mDa) | Relative mass error (ppm) | Observed accurate mass (Da) | Elemental formula | Calculated exact mass (Da) | Absolute mass error (mDa) | Relative mass error (ppm) |
| P1-245 | 245.1525 | C ₁₄ H ₂₂ O ₂ Na | 245.1517 | 0.8 | 3.3 | — ^b | | | | |
| P1-247 | 247.1326 | C ₁₃ H ₂₀ O ₃ Na | 247.1310 | 1.6 | 6.4 | 223.1341 | C ₁₃ H ₁₉ O ₃ | 223.1334 | 0.7 | 3.1 |
| P1-259 | 259.1681 | C ₁₅ H ₂₄ O ₂ Na | 259.1674 | 0.7 | 2.7 | — ^b | | | | |
| P1-261 | — ^b | | | | | 237.1494 | C ₁₄ H ₂₁ O ₃ | 237.1491 | 0.3 | 1.3 |
| P1-275 | 275.1628 | C ₁₅ H ₂₄ O ₃ Na | 275.1623 | 0.5 | 1.8 | 251.1646 | C ₁₅ H ₂₃ O ₃ | 251.1647 | -0.1 | -0.4 |
| P1-277 | 277.1422 | C ₁₄ H ₂₂ O ₄ Na | 277.1416 | 0.6 | 2.2 | 253.1447 | C ₁₄ H ₂₁ O ₄ | 253.1440 | 0.7 | 2.8 |
| P1-289 | 289.1431 | C ₁₅ H ₂₂ O ₄ Na | 289.1416 | 1.5 | 5.2 | 265.1476 | C ₁₅ H ₂₁ O ₄ | 265.1440 | 3.6 | 13.6 ^d |
| P1-291 | 291.1577 | C ₁₅ H ₂₄ O ₄ Na | 291.1572 | 0.5 | 1.6 | 267.1607 | C ₁₅ H ₂₃ O ₄ | 267.1596 | 1.1 | 4.1 |
| P1-305 | 305.1370 | C ₁₅ H ₂₂ O ₅ Na | 305.1365 | 0.5 | 1.7 | — ^b | | | | |
| P1-307 | 307.1516 | C ₁₅ H ₂₄ O ₅ Na | 307.1521 | -0.5 | -1.8 | 283.1554 | C ₁₅ H ₂₃ O ₅ | 283.1545 | 0.9 | 3.2 |
| P1-321 | 321.1308 | C ₁₅ H ₂₂ O ₆ Na | 321.1314 | -0.6 | -1.9 | 297.1345 | C ₁₅ H ₂₁ O ₆ | 297.1338 | 0.7 | 2.4 |
| P1-323 | 323.1465 | C ₁₅ H ₂₄ O ₆ Na | 323.1471 | -0.6 | -1.9 | 299.1492 | C ₁₅ H ₂₃ O ₆ | 299.1495 | -0.3 | -1.0 |
| P2-481 | 481.3298 | C ₂₉ H ₄₆ O ₄ Na | 481.3294 | 0.4 | 0.8 | — ^b | | | | |
| P2-497 | 497.3262 | C ₂₉ H ₄₆ O ₅ Na | 497.3243 | 1.9 | 3.8 | 473.3271 | C ₂₉ H ₄₅ O ₅ | 473.3267 | 0.4 | 0.9 |
| P2-511 ^c | 511.3337 | C ₃₀ H ₄₈ O ₅ Na | 511.3399 | -6.2 | -12.1 ^d | 487.3086 | C ₂₉ H ₄₃ O ₆ | 487.3060 | 2.6 | 5.3 |
| P2-513 | 513.3203 | C ₂₉ H ₄₆ O ₆ Na | 513.3192 | 1.1 | 2.1 | 489.3215 | C ₂₉ H ₄₅ O ₆ | 489.3216 | -0.1 | -0.2 |
| P2-527 | 527.3317 | C ₃₀ H ₄₈ O ₆ Na | 527.3348 | -3.1 | -5.8 | 503.3387 | C ₃₀ H ₄₇ O ₆ | 503.3372 | 1.5 | 3.0 |
| P2-543 | 543.3309 | C ₃₀ H ₄₈ O ₇ Na | 543.3298 | 1.1 | 2.0 | 519.3320 | C ₃₀ H ₄₇ O ₇ | 519.3322 | -0.2 | -0.4 |

1114 ^a Labels “P1-xxx” and “P2-xxx” denote P1 and P2 products having a nominal mass of xxx for their sodiated ions, respectively.1115 ^b Accurate mass was not measured because of the very low ion intensity or the strong interference from other ions such as impurities.1116 ^c Different formulae for P2-511 were identified in ESI+ and ESI- modes, which correspond, respectively, to aldol condensation products (P2-511-3 and P2-511-4) and esters (P2-511-1 and P2-511-2) as shown in Fig. 10c.1117 ^d The relatively large mass errors likely result from unknown interferences for P1-289 in ESI- mode and P2-511 in ESI+ mode. The
1118 given formulae are the closest to the observed masses but may not be correct because of the interferences.
1119